UNIVERSITAT DE BARCELONA

Escola de Camins
Escola Tècnica Superior d'Enginyeria de Camins, Canals i Ports
UPC BARCELONATECH

TREBALL FI DE CARRERA

Títol

Feasibility study on CO2 capture and storage in silicate substrates

Autor/a

Kwon Bok Rodriguez Rausis

Tutor/a

Ignasi Casanova Hormaechea

Departament

Department of Civil and Environmental Engineering

Intensificació

Carbon Capture and Storage

Data

July 2016

To my lovely wife Laura who touched my life. Sincerely yours.

Acknowledgments

There are many people I would like to thank, especially to Dr. Ignasi Casanova who introduce me to geoengineering CO_2 uptake technologies and guide me throughout this thesis development. I am grateful to Dr. Joaquim Proenza who provides the samples with a complete and specific characterization and gave support to this research. This work was supported by the CRnE (Centre for Research in NanoEngineering).

A special thanks to Agnieska Ćwik who collaborate with the experiment procedures, results interpretation and thesis assessing. To the CRnE Nanoparticles Staff, especially to Ander Elkoro who help me operate the FTIR transmission and support me with the interpretation of the results. Thanks also go to Dr. Montserrat Dominguez, who help to operate the XRD equipment and was very supportive towards laboratory practical issues. I acknowledge also the assistance of Dr. Albert Casanovas who support the carbonation experiment.

I am grateful to the UPC (Universitat Politècnica de Catalunya) and UB (Universitat de Barcelona) for all this unforgivable years of education.

I like to thank prof. Xavier Couto who taught me in detail AutoCAD.

Unique thanks goes to my wife Laura Couto who has always being there to support me in the whole development of this research.

Finally, very special thanks to my family who have always encourage me to study, and they have always been very supportive in all aspects.

Abstract

The increasing CO_2 concentrations in the atmosphere are attributed to the rising consumption of fossil fuels for energy generation. Mineral carbonation technologies methods are needed to prevent the global warming bellow 2ºC at the end of this century proposed in the Paris summit 2015. Carbonates mineralization of peridotites and serpentines can be enhanced in order to develop a significant method to safety storage CO_2. These minerals have been proved to have higher affinity towards sinking of CO_2. The goal of this thesis is the feasibility study of the carbonation reaction in typical mantel peridotites and serpentines. Specific experimental conditions were defined by reproducing the ones that gave the greater CO_2 uptake with lower energy required cost, published at Kelemen and Matter, 2008. The samples where grounded to powder and exposed to a gas solid interaction at 185ºC and 1 bar of CO_2 pressure plus atmospheric pressure for 2 hours. Under these conditions, all the samples had an increase in the carbonates proportion and it was clearly determined by using the following methods: powder XRD, FTIR transmission and acid triggered de-carbonation. FTIR results revealed clearly the changes caused by the carbonation reaction, giving the most accurate carbonation formation response. The latter also revealed qualitatively the increase of magnesite proportion in all the samples. The acid triggered experiment results revealed that the CO_2 uptake by mineral carbonation reached a maximum value of 4%. Nevertheless, any of the methods could give a quantitative precise carbonation rate. The peridotites samples in all methods show a clear carbonation trend. The comparison between the peridotites samples composition and the carbonation rate estimated revealed the inverse relation of Mg# and Ca# towards CO_2 uptake. At higher Mg# greater the carbonation rate. The Dunite sample (LT-1) carbonated the most out of the peridotites samples, which is the sample that has the highest Mg# and the lower Ca#. XRD results reveal that all the peridotites samples had calcium carbonate formation. Serpentines showed complex results that can be attributed to their mineral and compositional complexity.

Resumen

El incremento de la concentración de CO_2 en la atmósfera es atribuido al elevado consumo de combustibles fósiles para la generación de energía. Las tecnologías de carbonatación mineral son necesarias para prevenir que el calentamiento global supere los 2ºC para el final de este siglo, propuesto en el Paris Summit 2015. La carbonatación de peridotitas y serpentinas puede ser acelerada a tal punto de ser considerado como un significante método para capturar CO_2. Se ha probado que estas rocas tienen una alta afinación en almacenar seguramente el CO_2. El objetivo de esta tesina es el estudio de viabilidad de la reacción de carbonatación en peridotitas y serpentinas. Las condiciones de este estudio fueron definidas según los resultados que dieron la mayor captura de CO_2 con el menor coste energético según el estudio de Kelemen and Matter, 2008. Las muestras fueron molidas y expuestas a una interacción de gas y sólido a 185ºC y una presión de 1 bar de CO_2 más la presión atmosférica por dos horas. Bajo estas condiciones, todas las muestras presentaron un aumento en la proporción de carbonatos y fue claramente determinado utilizando los siguientes métodos: Difracción de polvo cristalino XRD, FTIR de transmisión y de-carbonatación por ácido. Los resultados de FTIR revelaron claramente los cambios causados por la reacción de carbonatación, dando la respuesta más precisa en cuanto a formación de carbonatos. Estos resultados también revelaron de forma cualitativa el incremento de proporción de magnesita en todas las muestras. Los resultados de de-carbonatación por ácido revelaron que el máximo de captura de CO_2 obtenido en todas las muestras es del 4%. Sin embargo, ninguno de los métodos pudo dar una cuantitativa tasa de carbonatación. Las muestras de peridotitas en todos los métodos mostraron una clara tendencia de carbonatación. La comparación entre la composición y la tasa de carbonatación para las muestras de peridotitas revela la inversa relación del Mg# y Ca# en la captura de CO_2. A grandes valores de Mg# mejor su tasa de carbonatación. La muestra de Dunita (LT-1) presenta la mayor tasa de carbonatación entre las muestras de peridotitas, la cual es la muestra que tiene el mayor Mg# y el menor Ca#. Los resultados de XRD revelaron que todas las muestras de peridotitas han formado carbonato de calcio. Las serpentinas mostraron resultados complejos los cuales pueden ser atribuidos a su complejidad mineral y composicional.

Key Words

- BECCS: Bioenergy with Carbon Dioxide Capture and Storage
- CDR: Carbon Dioxide Removal
- CCS: Carbon Capture and Storage
- CRnE: Centre for Research in NanoEngineering
- FTIR: Fourier Transform Infrared Spectroscopy
- GHG: Greenhouses Gases
- IEA: International Energy Agency
- IPCC: Intergovernmental Panel on Climate Change
- LOI: Loss On Ignition
- OECD: Organisation for Economic Co-operation and Development
- PL: Passivating Layer
- RE: Renewable Energy
- RF: Radiative Forcing
- XRD: X-Ray Powder Diffraction

Table of Contents

List of Figures

- **Fig. 17.** X-Ray Powder Diffraction spectrum results before and after carbonation for every sample superposed, focused on the area of 100 peak characteristic of carbonates. (A) LT-1, (B) LT-3, (C) LT-4, (D) C-626-9, (E) 14-SC-7, (F) 09-LV-IIA.
- **Fig. 18.** FTIR Transmission spectrum result focused on the carbonated absorption band and main changes between the samples before carbonated, with their correspondent base line which will be used to compare the area changes between both spectrums for each sample. (A) LT-1, (B) LT-3, (C) LT-4, (D) C626-9-, (E) 14-SC-7, (F) 09-LV-IIA.
- **Fig. 19.** Comparison between the mass loss % of the samples and the (Left) Ca# with a three-parameter logarithm function (Log3P1) and (Right) Mg# with a two-parameter logarithm function (Log2P2). The non-linear curves were calculated with OriginLab 8. Green: Peridotites samples, Red: Serpentines samples.
- **Fig. 20.** Comparison between the V4 absorbance normalized area of the samples after carbonation and the (Left) Ca# with a two parameter exponential function (Exp2P) and (Right) Mg# with a three parameter exponential function (Exp3P2). The non-linear curves were calculated with OriginLab 8. Green: Peridotites samples, Red: Serpentines samples.

Appendix A

- **Fig. A 1.** Results of the X-Ray Powder Diffraction analysis from $2\theta = 10^{o} - 40^{o}$ and interpretation of the peridotites samples; S: Serpentine, O: Olivine, P: Clinopyroxene, E: Orthopyroxene, D: Dolomite; C: Calcite, M: Magnesite, B: Brucite.
- **Fig. A 2.** Results of the X-Ray Powder Diffraction analysis from $2\theta = 10^{o} - 60^{o}$ and interpretation of the Serpentine samples; S: Serpentine, O: Olivine, C: Calcite; M: Magnesite; D: Dolomite. The peak counts for the sample 09-LV-IIA are much higher than the ones from 14-SC-7.
- **Fig. A3.** Results of the X-Ray Powder Diffraction analysis from $2\theta = 10^{o} - 40^{o}$ targeting the 100 peaks for Carbonates, Serpentine and Silicates of the LT-1 samples before and after carbonation. S: Serpentine, O: Olivine, D: Dolomite; C: Calcite, M: Magnesite, B: Brucite.
- **Fig. A4.** Results of the X-Ray Powder Diffraction analysis from $2\theta = 10^{o} - 40^{o}$ targeting the 100 peaks for Carbonates, Serpentine and Silicates of the LT-3 samples before and after carbonation. S: Serpentine, O: Olivine, E: Orthopyroxene, D: Dolomite; C: Calcite, M: Magnesite.
- **Fig. A5.** Results of the X-Ray Powder Diffraction analysis from $2\theta = 10^{o} - 40^{o}$ targeting the 100 peaks for Carbonates, Serpentine and Silicates of the LT-4 samples before and after carbonation. S: Serpentine, O: Olivine, P: Clinopyroxene, E: Orthopyroxene, D: Dolomite; C: Calcite, M: Magnesite.
- **Fig. A6.** Results of the X-Ray Powder Diffraction analysis from $2\theta = 10^{o} - 40^{o}$ targeting the 100 peaks for Carbonates, Serpentine and Silicates of the C-626-9 samples before and after carbonation. S: Serpentine, O: Olivine, P: Clinopyroxene, E: Orthopyroxene, D: Dolomite; C: Calcite, M: Magnesite.
- **Fig. A7.** Results of the X-Ray Powder Diffraction analysis from $2\theta = 10^{o} - 40^{o}$ targeting the 100 peaks for Carbonates, Serpentine and Silicates of the 14-SC-7 samples before and after carbonation. S: Serpentine, D: Dolomite; C: Calcite, M: Magnesite.

- **Fig. A8.** Results of the X-Ray Powder Diffraction analysis from 2θ = 10º - 40º targeting the 100 peaks for Carbonates, Serpentine and Silicates of the 09-LV-IIA samples before and after carbonation. S: Serpentine, D: Dolomite; C: Calcite, M: Magnesite.

Appendix B

- **Fig. B1.** FTIR transmission spectrum result of the sample LT-1 before and after carbonated. The V indicates the peaks use for comparison, and the base line determines the area to be calculated.
- **Fig. B2.** FTIR transmission spectrum result of the sample LT-3 before and after carbonated. The V indicates the peaks use for comparison, and the base line determines the area to be calculated.
- **Fig. B3.** FTIR transmission spectrum result of the sample LT-4 before and after carbonated. The V indicates the peaks use for comparison, and the base line determines the area to be calculated.
- **Fig. B4.** FTIR transmission spectrum result of the sample C-626-9 before and after carbonated. The V indicates the peaks use for comparison, and the base line determines the area to be calculated.
- **Fig. B5.** FTIR transmission spectrum result of the sample 14-SC-7 before and after carbonated. The V indicates the peaks use for comparison, and the base line determines the area to be calculated.
- **Fig. B6.** FTIR transmission spectrum result of the sample 09-LV-IIA before and after carbonated. The V indicates the peaks use for comparison, and the base line determines the area to be calculated.

List of Tables

1. State of the art

1.1. Evidence of Climate Change

The Intergovernmental Panel on Climate Change (IPCC) has clearly shown the relation between global warming and the recent anthropogenic emissions of greenhouses gases (GHG) to the atmosphere, reaching the highest concentrations ever recorded in the history. The impact of human beings is clear and evident, the global warming is **Unequivocal**, the atmosphere and the ocean have warmed; the amounts of snow and ice have diminished, and see level has risen (IPCC, 2014).

The concentration of GHG has increased since the pre-industrial era, being the motor of the society as we know our days. This has led to a GHG concentration increase on the atmosphere to that correspondent to 800,000 years ago. Since 1750 to 2011 total cumulative Carbon Dioxide (CO_2) emitted to the atmosphere were 2040 ± 310 Gigatones (Gt) (Fig. 1.), about 40% of this gases remained in the atmosphere that corresponds to 880 ± 35 Gt; the other 60% was removed from the atmosphere and mainly captured in Oceans (around 30% of the total CO_2 accumulative emitted, causing the ocean acidification by decreasing the PH of the ocean in 0.1), plants and soils. The emissions are in continuous growth, about 50% of the total accumulative CO_2 emitted since 1750 until 2011 have occurred in the last 40 years (IPCC, 2014).

There is evidence in the continues increasing global warming in the last three decades successively at the Earth`s Surface, making it, the warmest three successive decades on the last 1400 years (Fig. 1). Ocean warming accumulates the 90% of the energy stored in the climates systems over the period 1971 until 2010, and just 1% is stored in the atmosphere (IPCC, 2014).

Despite the large amount of climate change mitigation policies around the world, the CO_2 emission rate is increasing faster from 1970 until 2010 , especially in the last 10 years. The 78% of these emissions proceed from fossil fuel combustion and industrial processes over the period 1970 until 2010. The population is in continuous growth, and also the demand of energy required, those are the most important drivers of the increase of CO_2 emissions. As IPCC fifth Assessment Report express: it is extremely likely that more than the half of the observed increase in global average surface temperature from 1951 to 2010 was caused by anthropogenic increase in GHG concentrations and other anthropogenic forcing together (IPCC, 2013). (Fig. 1 c, d)

The analysis of the total Radiative Forcing (RF) is a very precise method that analyses the effect of the anthropogenic effects and its direct relation with the global warming. Their units are watts per square meter (W m^{-2}) and measure the change of energy flux cause by a driver, and it's calculated at the tropopause. A positive RF indicates possible surface warming and negative RF indicates possible surface cooling. The total anthropogenic RF measured from 1750 until 2011 is 2.29 W $m^{-2,}$ and emissions of CO_2 alone contributes with an RF of 1.82, making it the most important gas of the GHG that drives the global warming (Fig. 2). Controlling the CO_2 emissions and dealing with CO_2 accumulated in the atmosphere is one of the main objectives to mitigate effects of the global warming. . Many technologies such as Conservation and Energy

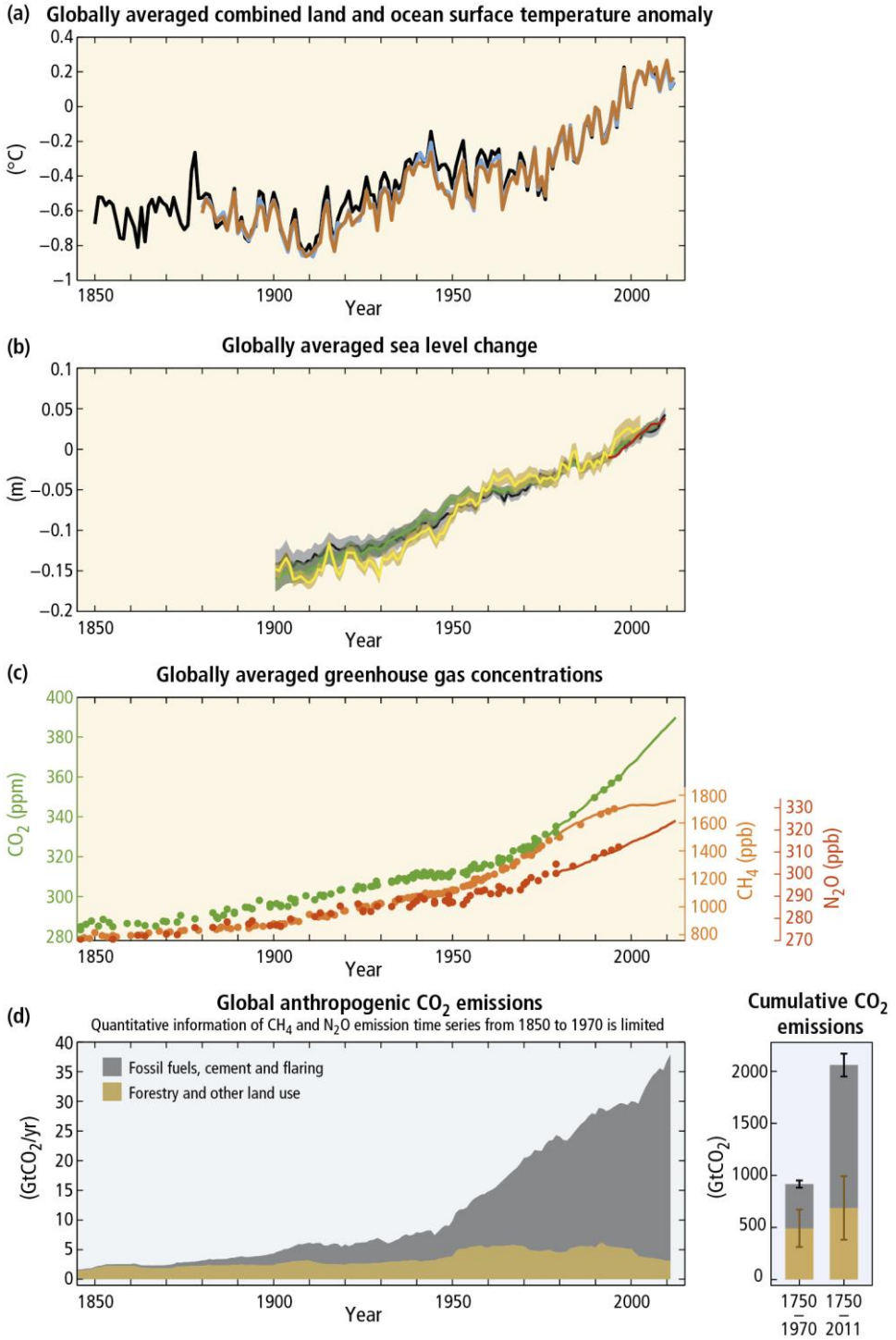

Fig. 1. Relation between the increasing temperature and the sea level rising since 1850 until 2010 as a result of the increasing greenhouse gases concentration specific to the global anthropogenic CO_2. **(a)** Anomalies of the combined land and ocean's surface temperature relative to the average over the period 1986 to 2005. This data is calculated by a linear trend show a warm of 0.85 $°C^2$ over the period 1880 to 2012. **(b)** Raising of the sea level relative to the average over the period 1986 to 2005. Global mean see level rose by 0.19m over the period 1901 to 2010. **(c)** Increasing of the concentrations of the greenhouses gases (CO_2, Methane (CH_4) and Nitrous Oxide (N_2O)) determined from ice core data (dots) and from direct atmospheric measurements (lines). **(d)** To the left, Global anthropogenic CO_2 due to forestry and other land use as well as from burning fossil fuels, cement and flaring emissions rate per year. To the right, Cumulative CO_2 emissions from this sources and uncertainties. Notice the greater increased in the cumulative CO_2 from 1970 until 2011 to the one from 1750 until 1970 (IPCC, 2014).

Efficiency, Renewable Energy (RE), Nuclear Energy, Coal and Gas Substitution and **Carbon Capture and Storage (CCS)**, have to develop in order to meet the increasing demand of energy that our growing population requires our days and to mitigate their emissions of GHG, and to meet the projected demand of energy and growing population on short to long term and their projected emissions of GHG (IPCC, 2013).

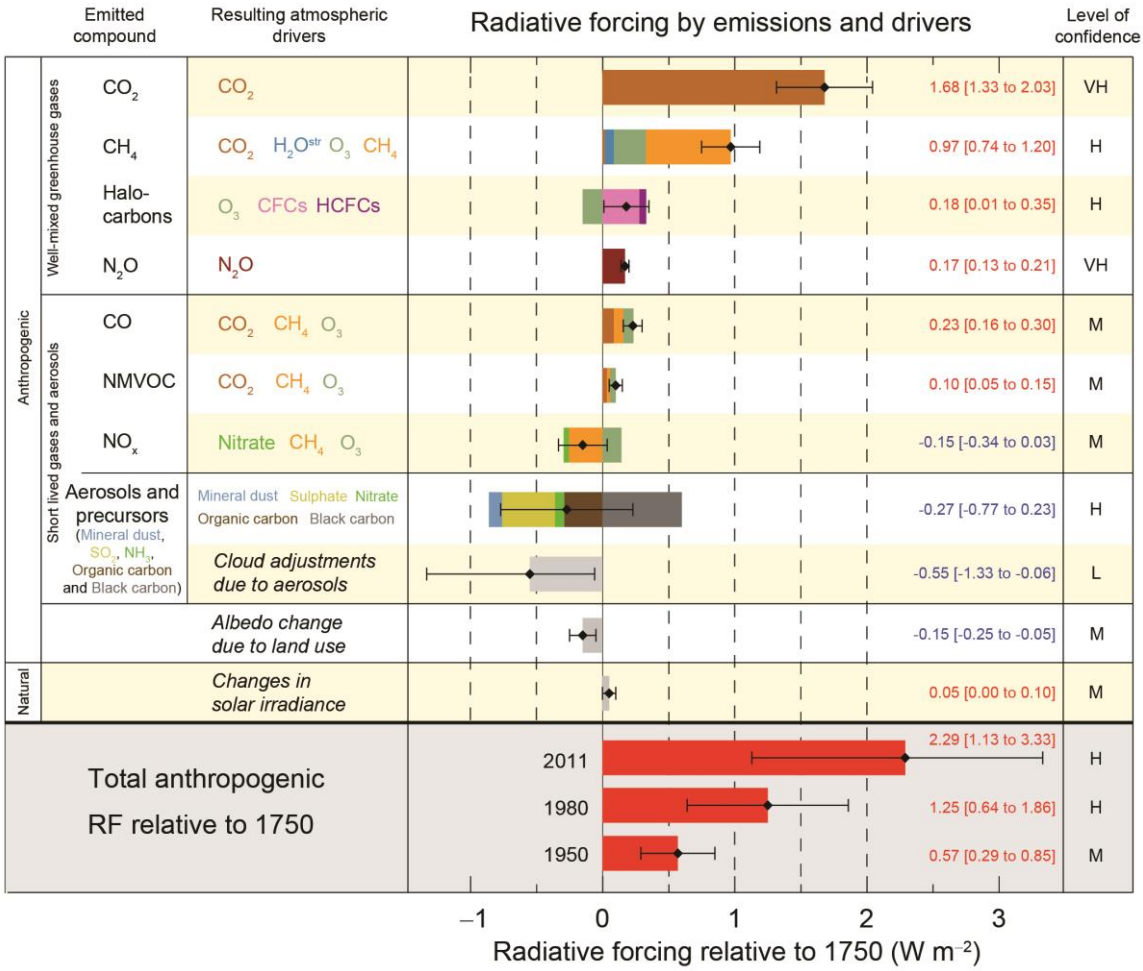

Fig. 2. RF estimated over the period from 1750 until 2011, adding the uncertainties in whiskers shape. Volcanic forcing is not included as its episodic nature makes is difficult to compare to other forcing mechanisms. The confidence level means are shown as: VH – *Very High*, H – *High*, M – *Medium*, L – *Low*, VL – *Very L*. Notice the increasing RF on the last three decades, which is much higher than the one presented from 1950 to 1980 (IPCC, 2013).

The total RF natural generated, related to the changes in solar irradiance is 0.05 W m^{-2}, comparing it with the total RF anthropogenic, is almost unappreciable (Fig. 2).

1.2. CCS and its importance to mitigate the CO_2 emissions.

"Without additional mitigation efforts beyond those in place today, and even with adaptation, warming by the end of the 21st century will lead to high to very high risk of severe, wide-spread and irreversible impacts globally (high confidence[1]) (IPCC, 2013).

In a scenario with the efforts that are placed today to mitigate the emissions of GHG, the increasing growth rate is expected to keep growing, the projected increment of temperature at the end of 21st century is expected to be on a range of 3.7 °C and 4.8 °C (without introducing uncertainties). This is clear evidence that there is a global need to create pathways and policies that project a progressive mitigation of GHG emissions.

For this reason, the IPCC fifth Assessment Report proposes different scenarios where GHG emissions are strictly controlled in order to generate a possible pathway to mitigate global warming. The scenarios that are most likely to maintain global warming below 2 °C are characterized by 40 to 70% of GHG emissions reduction by 2050 compared to 2010, and reaching a CO_2-equivalent concentration in 2100 of about 450 ppm, with reliance on Carbon Dioxide Removal (CDR), or characterized by 25 to 55% of GHG emissions reduction by 2050 compared to 2010, and reaching a CO_2-equivalent concentration in 2100 of about 500 ppm concentration with a strong reliance on CDR (IPCC, 2013). These scenarios will require the emissions of no more than 880 Gt of carbon, which is the global carbon budget, and 530 Gt of them has already being consumed in 2011 (Willis et al., 2014). But meeting it won´t be easy, given that we are currently on track for between 4 °C and 5 °C. Our only hope is to decisively pick up the pace (Mckibben, 2015).

This scenarios can only be reached by increasing form the current 30% to more than 80% by 2050 the use of low-carbon electricity supply, which consist on RE, nuclear energy and CCS (including bioenergy with carbon dioxide capture and Storage (BECCS), and fossil fuel power generation without CCS is phased out almost entirely by 2100. Many models cannot reach 450ppm CO_2-eq concentration by 2100 in the absence of CCS (IPCC, 2014). Many models guarantee most likely that without CCS the global warming could not limit bellow 2°C over the 21st century relative to pre-industrial levels, and its availability would reduce the adverse effect of mitigation on the value of fossil fuel assets (Medium confidence), without CCS the costs of climate change mitigation would increase by 138 per cent (IPCC, 2014).

CCS technology is proven and in use around the world. It has a key role to play in curbing CO2 emissions from fossil fuel based power generation, which will experience continued growth, especially in Asia (Global CCS institute, 2015). We are running out of time, and we need to take action fast. As the International Energy Agency (IEA) affirm in the CCS Technology Roadmap, 2013 (IEA, 2013b), we need to support, encourage, prove and develop CCS technologies in the next 7 years through a 7 key action, in order to achieve the low-carbon stabilization goals. Also affirms that CCS is the only large-scale project with the capacity to reduce CO_2 emissions from industrial sectors. Failure to utilize CCS technology in industrial

[1] The IPCC expresses the degree of uncertainty as a qualitative level of confidence (from *very low* to *very high*) and, when possible, probabilistically with a quantified likelihood (from *exceptionally unlikely* to *virtually certain*) (IPCC, 2013).

applications poses a significant threat to the world's capacity to tackle climate change (IEA, 2013a).

According to IEA modeling, the total cumulative emissions reductions by 2050 that the CCS could deliver is 13% which is needed to achieve the 2°C scenario, generating an expected capacity of about 6,000 million tons of CO_2 ($MtCO_2$) per year by 2050. (IEA, 2015a) (Fig. 3)

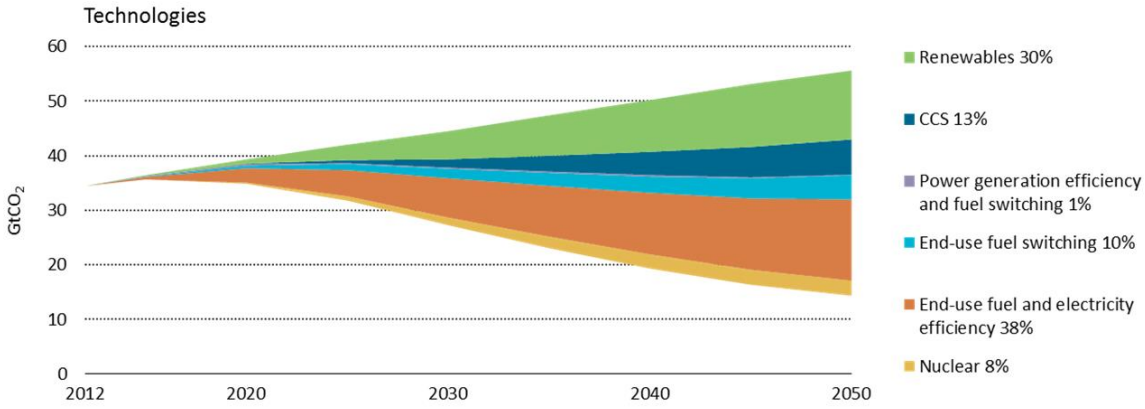

Fig. 3. Expected Contributions of technologies and sectors to global cumulative CO2 reductions based on the IEA's Modelling. CCS technologies is projected to safety captured a 13% of the total emission reduction by 2050 (IEA, 2015a).

To achieve the goal of limiting the global warming increases to no more than 2°C, an enormous deployment of low-carbon technologies is needed in all sectors. Nowadays, there is 15 large scales CCS project that are currently operating, with the capacity to capture 28 million tons of CO_2 per year (IEA, 2013a). But this is not enough, it is necessary that by the 2040 the capacity of the large-scales CCS projects needs to increase up to 4,000 $MtCO_2$ per year and by 2050 needs to increase up to 6,000 $MtCO_2$ per year (IEA, 2015b). By 2020, a total amount of 30 large-scale operating CCS projects is expected (IEA, 2013a) (Fig. 4).

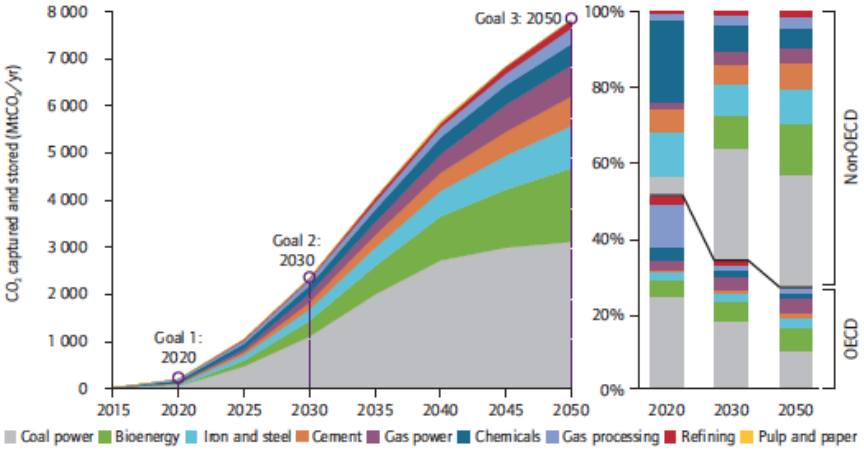

Fig. 4. Goals for CCS in the power and industrial sectors in order to achieve the 2 °C scenario. Notice that the Goal 3 proposes an increase of the capacities of the CCS projects reaches a total of 8,000 MtCO2 per year. Over 70% of all CCS projects take place in non-Organisation for Economic Co-operation and Development (OECD) countries by 2050 (IEA, 2013b).

This goals are only achievable if the price of Carbon Dioxide reductions would have to exceed 25-30 US$/t$CO_2$, or an equivalent limit of CO_2 emissions would have to be mandated (IPCC, 2005). Current prices in the EU are too low to make CCS attractive to investors (Neslen, 2015). This technology still needs to develop in order to make it happen, and many experimental essays at pilot scales are needed to improve our knowledge and security in CCS.

A nearly two mile fracture has already been found close to the Sleipner carbon repository. But the CO_2 there will have to be kept underground for many centuries and not just to prevent climate change (Neslen, 2015). One way to keep the captured CO_2 in the ground is to change its gas phase to solid phase through mineral carbonation technology, which can reduce costs and energy requirements due to the produced heat reaction (IPCC, 2005).

1.3. Mineral Carbonation for CO_2 storage.

The alteration of tectonically exposed mantle peridotite is well known as sink for atmospheric CO_2. Weathering and subsequent precipitation of calcium- and magnesium-carbonates is the main mechanism by which the CO_2 levels of the atmosphere are controlled (Schuilling and Krijgsman, 2006). The natural rate of the reaction between peridotite and CO_2 (mineral carbonation) is very slow and is usually drive by low temperatures and weathering conditions. This natural rate can be enhanced through increasing the kinetics of the carbonation reaction becoming a significant sink of CO_2. In order to increase the kinetics of carbonation reaction an initial heating step in the hosting bulk is required, this generates exothermic reactions that heat the CO_2 incoming. Temperatures necessary for rapid reaction can be sustained via exothermic carbonation, instead of an external heat source. The kinetics is enhanced and the cost of energy is relatively low due to the energy cost rely in just an initial heating step. By this method it is expected that in situ carbonation of peridotite could consume >1 billion tons of CO_2 per year in Oman alone (Kelemen and Matter, 2008).

In order to optimize the storage capacity it is needed to find the rock type and mineral composition that has the largest CO_2 storage capacity. Olivine, which is the Dunite main component, is the mineral that has the most affinity towards mineral carbonization of CO_2, and its sinking minerals are mainly magnesite and siderite. During the hydration and carbonation reactions, the silicate bulk gets Fe-rich (Streit et al., 2012)), but this rock is not stable in crustal conditions (Xu et al., 2004), reacting with H_2O and CO_2 present in in crustal conditions to form serpentine and carbonates and Fe-Oxides.

The main reactions that show the CO_2 storage potential are formulated as follows (Klein and Garrido, 2011; Gerdemann et al., 2003):

$$\underset{\text{Mg}-\text{Olivine}}{2Mg_2SiO_4} + \underset{\text{Mg}-\text{Pyroxene}}{Mg_2Si_2O_6} + 4H_2O \underset{\text{Hydratation}}{=} \underset{\text{Serpentine}}{2Mg_3Si_2O_5(OH)_4} \quad (1)$$

$$\underset{\text{Mg}-\text{Olivine}}{2Mg_2SiO_4} + CO_2 \underset{\text{Carbonation}}{=} \underset{\text{Magnesite}}{2MgCO_3} + \underset{\text{Quartz}}{SiO_2} \quad 10.3\ \text{Kcal} \tag{2}$$

$$\underset{\text{Mg}-\text{Olivine}}{2Mg_2SiO_4} + \underset{\text{Ca}-\text{Mg}-\text{Pyroxene}}{CaMgSi_2O_6} + 2CO_2 + 2H_2O \underset{\text{Carbonation}}{\overset{\text{Hidratation}}{=}} \underset{\text{Serpentine}}{2Mg_3Si_2O_5(OH)_4} + \underset{\text{Calcite}}{CaCO_3} + \underset{\text{Magnesite}}{MgCO_3} \tag{3}$$

$$\underset{\text{Serpentine}}{2Mg_3Si_2O_5(OH)_4} + 3CO_2 \underset{\text{Carbonation}}{=} \underset{\text{Magnesite}}{3MgCO_3} + \underset{\text{Quartz}}{2SiO_2} + 2H_2O \tag{4}$$

Equations (1), (2), (3) and (4) are exothermic because Serpentine and Magnesite are at a lower thermodynamic state than olivine (Klein and Garrido, 2011). For this reason, over geologic time olivine reacts with very low kinetics, and is eventually converted into serpentine and magnesite. As a consequence, serpentine and magnesite are more abundant than Olivine near Earth Surface (Gerdemann et al., 2003).

Evidence of natural hydration and carbonation at low-temperatures can be found in springs and associated travertines. The Samail Ophiolite is a good example of it, which is an uplifted slice of the oceanic crust (Kelemen and Matter, 2008). The ultramafic rocks at Atlin represents a tectonically emplaced upper mantle section of oceanic lithosphere composed of hazburgite and dunite, that is mostly converted into serpentine and listwanite (Hansen et al., 2005).

Another natural evidence can be found in the transform fault in the Atlantic oceanic ridge located at latitude 15º20'N, which has been drilled and analyzed. The 1274A Drill shows an almost fully serpentinized peridotite, from 60 to 100%. The serpentinization of Olivine generates a mesh texture, starting from the edges of the pre-Olivine mineral to the center (full serpentinization) It is very common to find Olivine in the core of the mineral that is being serpentinized and serpentine (Lizardite) conforming the mesh texture. Later, the olivine core has being replaced by a second generation serpentine and brucite (Garrido et al., 2006).

There is a large amount of CO_2 that has to be captured and storage indefinitely, because a small re-release of CO_2 will quickly equal the release from burning fossil fuels (Gerdemann et al., 2003). This storage request can be accomplished when carbonate (magnesite and siderite mainly) is formed out of the carbonation reaction of peridotites.

The affinity that olivine, pyroxene, wolframite, serpentine and others have with CO_2 can be explained by the fluids related to them at low temperatures (alkaline, Ca-rich and Mg-rich). In the process of serpentinization a breakdown from their silicate precedent occurs, increasing the Ca^{2+} and Mg^{2+} concentration in the fluid. The loss of Ca^{2+} and Mg^{2+} is reflected by the Ca and Mg depletion observed in many serpentinized peridotites (Frost and Beard, 2007).

$$\underset{\text{Diopside}}{3CaMgSi_2O_5} + 3H^+ \underset{\text{Serpentinization}}{=} \underset{\text{Serpentine}}{Mg_3Si_2O_5(OH)_4} + \underset{\text{Quartz}}{4SiO_2} + H_2O + Ca^{2+} \quad (5)$$

At low CO_2 concentrations, the hydration reaction generates serpentine and liberates Mg^{2+} which forms brucite.

$$\underset{\text{Mg}-\text{Olivine}}{2Mg_2SiO_4} + 3H_2O \underset{\text{Hydration}}{=} \underset{\text{Serpentine}}{Mg_3Si_2O_5(OH)_4} + \underset{\text{Brucite}}{Mg(OH)_2} \quad (6)$$

When Olivine is completely converted, the hydration of serpentine to brucite and silica starts (Frost and Beard, 2007):

$$\underset{\text{Serpentine}}{Mg_3Si_2O_5(OH)_4} + H_2O \underset{\text{Hydration}}{=} \underset{\text{Brucite}}{3Mg(OH)_2} + \underset{\text{Quartz}}{2SiO_2} \quad (7)$$

At low temperatures modest concentrations of CO_2 would be sufficient to dissolve brucite in favor of carbonate (Klein and Garrido, 2011).

$$\underset{\text{Brucite}}{3Mg(OH)_2} + CO_2 \underset{\text{Carbonation}}{=} \underset{\text{Magnesite}}{3MgCO_3} + 2H_2O \quad (8)$$

The equation 5 shows that when the silica activity decreases, caused by the falling temperatures, the Ca^{2+} activity increases more than three orders of magnitude, and pH will rise (Fig. 5) (Frost and Beard, 2007). The serpentinized reaction stars when the low silica activity compromises the stability of components in olivine, such as the ferrous iron, which goes to the formation of magnetite. Serpentine is more silica rich than olivine, so without an external input of silica it must coexist with a less silica-rich Mg phase, such as magnesite, dolomite or brucite. At higher CO_2 partial pressure the rate of carbonate precipitation increase, which raises the silica activity of the fluid (Streit et al., 2012). The instability of pyroxene and olivine at low silica activity results in its incongruent dissolution, producing the Ca-rich fluids associated with serpentinization (Frost and Beard, 2007). The carbonate is believed to precipitate when Ca-rich and high pH serpentinization fluids mix with bicarbonate-rich seawater (Klein and Garrido, 2011).

When silica activity levels are high in presence of serpentine, this reacts to form talc (Equation 9) (Frost and Beard, 2007). Full carbonation of serpentine or olivine is achieved when all the talc has reacted to form magnesite and quartz (10) (Klein and Garrido, 2011).

$$\underset{\text{Serpentine}}{Mg_3Si_2O_5(OH)_4} + \underset{\text{Quartz}}{2SiO_2} = \underset{\text{Talc}}{Mg_3Si_4O_{10}(OH)_2} + H_2O \quad (9)$$

$$\underset{\text{Talc}}{Mg_3Si_4O_{10}(OH)_2} + 3CO_2 \underset{\text{Carbonation}}{=} \underset{\text{Magnesite}}{3MgCO_3} + \underset{\text{Quartz}}{4SiO_2} + H_2O \quad (10)$$

At low temperatures, chemical potential gradients of silica and CO_2 activities between the fluid of serpentine-brucite reactions and the fluid of CO_2 rich, talc-SiO_2-magnesite are increased, but mineral carbonation is limited (Klein and Garrido, 2011). In increased temperatures higher CO_2 activity is needed for carbonation of serpentine (Klein and Garrido, 2011). The temperature of mineral carbonation is of great importance as reaction rates are sluggish at very low and high temperatures (Klein and Garrido, 2011). Optimal temperature for mineral carbonation of heat-treated serpentine with CO_2 saturated aqueous fluid is 155 °C (Gerdemann et al., 2003; Klein and Garrido, 2011).

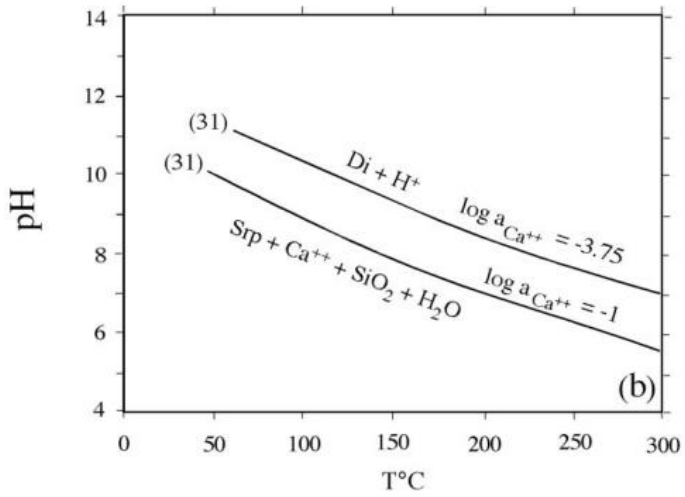

Fig. 5. Stability of Diopside in serpentine. pH vs Temperature diagram showing how the solution of Diopside of the serpentine-brucite buffer produces progressively more alkali fluids with decreasing temperature. The reaction (31) is referred in this work as equation (5) (Frost and Beard, 2007).

Notice that the reactions shown in equation (1), (2), (4), (5), (7) and (10) contributes to an increasing of silica activity, which can be precipitated as amorphous pure silica, leading to the presence of unreacted olivine at the core. When the carbonation reaction occurs, the aqueous olivine carbonations process involves magnesium dissolutions and silica precipitation (Fig. 6) (Chizmeshya et al., 2007), generating Silica-rich reaction layers and surface regions missing glasslike layer fragments, referred as passivating layers (Béarat et al., 2006). This silica is mainly generated by the reaction of olivine alteration to serpentine and/or magnesite (Klein and Garrido, 2011), as the result of incongruent carbonation of silicates and can also be generated by talc (Streit et al., 2012). This layer is highly stressed due to the large molar volume difference between SiO_2 and olivine, this produce fractures and exfoliations.

Silica-rich passivating layer act as a barrier covering the olivine mineral, and inhibit the interaction between olivine and the rich fluids and gases. By this reason, it substantially inhibit mineral carbonation reactivity (Béarat et al., 2006). Sonication has being applied to the samples that has a passivating layer formed in order to remove it, but none of the methods had have a significant carbonation improvement in removing the silica content (Chizmeshya et al., 2007).

These processes occurs natural at very low reaction kinetics. In order to be able the generate a technology that can storage safety large amount of CO_2 in very short time it is needed to accelerate the kinetics of this reactions, which has a direct implication on their costs.

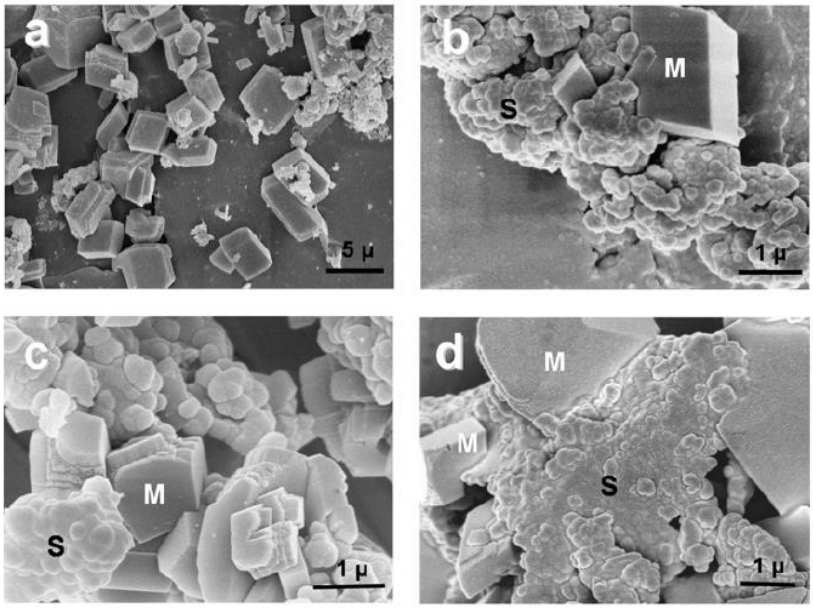

Fig. 6. FESEM images of olivine carbonation reaction products. Two types of particles are observed, crystals and irregularly shaped particles. The products are most often observed as separate particles and crystals, but are also observed to have aggregated into clusters during the mineral carbonation process. (a, b) magnesite crystals (M) and irregularly shaped silica-rich particles (S). Magnesite crystals with eroded edges and corners are often observed, suggesting substantial particle abrasion occurs during carbonation. (d) A close up of an intergrowth silica/magnesite composite particle. Selective abrasion of the outer perimeter of the softer magnesite crystals, as observed for the two crystals in the upper left corner, indicates intergrowth particles from during carbonation and not as the result of precipitation (Chizmeshya et al., 2007).

The reaction rate can be accelerated by raising the temperature and pressure of the peridotite, injecting CO_2 rich fluids which changes the solution chemistry (Kelemen and Matter, 2008; Gerdemann et al., 2003; Klein and Garrido, 2011), decreasing particles size and using a catalyst (Kelemen and Matter, 2008; Gerdemann et al., 2003; Klein and Garrido, 2011; Rigopoulos et al., 2015a, Rigopoulos et al., 2015b). Heating and raising the partial pressure of CO_2 can increase the carbonate rate by a factor of $>10^6$ (Fig. 7), with a potential increase up to 10^9 by continuous induced fracturing on the bulk during the process (Kelemen and Matter, 2008). All of these approaches improve reaction kinetics, increasing greatly its rate, making possible accelerating the formation of carbonate to conversions of over 80% in less than an hour, but this improvement carry energy and economic costs (Gerdemann et al., 2003). As a consequence understanding the hydration and carbonation reactions of peridotite can constrain the optimal conditions and limitations of CO_2 sequestration.

Hydration and carbonations reactions generate volume changes due to consumption of CO_2 to form solid Magnesite. Carbonation of Olivine result in 44% increase in the solid volume, this lead to enormous pressure increases and fracture may be anticipated (Kelemen and Matter, 2008).

Increasing the temperature and partial pressure accelerates the kinetics of the hydration and carbonation reaction until temperature approaches the equilibrium phase boundary for carbonate and serpentine mineral stability. Over a range of temperatures the reaction rate of serpentinization has a maximum level at 260 °C, and carbonation is optimized at 185 °C and 150 bar CO_2 pressure (Fig. 7) (Kelemen and Matter, 2008). Overpassing the optimized reaction rates by increasing temperature mainly produce a decrease in CO_2 dissolution and the reaction becomes thermodynamically less favorable (Gerdemann et al., 2003).

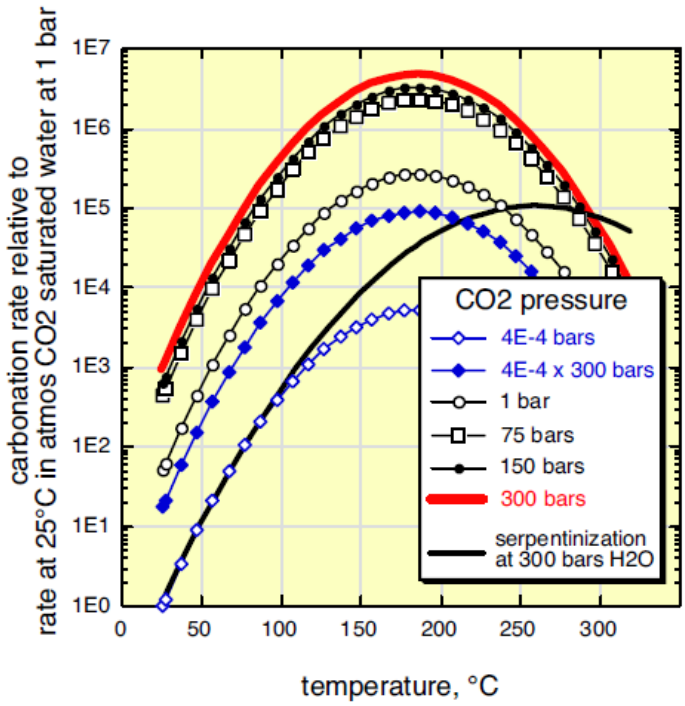

Fig. 7. Rate of olivine carbonation (lines and symbols) and serpentinization (black line, no symbols) as a function of temperature and pressure, compared with the rates at 25°C for surface water equilibrated with the atmosphere at 1 bar. A range of curves are shown for carbonation, with a single curve for serpentinization of olivine saturated in aqueous fluid at 300 bars (Kelemen and Matter, 2008).

Reaction rate is clearly higher for carbonation than serpentinization (Fig. 7). This is because the enthalpy change is 3 times larger for carbonation, for example, at 1 bar and 25 °C, the heat produced due to serpentinization is ΔH is 250kJ/kg, and for carbonation can reach ΔH of 760 kJ/kg, and sepentinization is slower than carbonation in the range of optimized conditions shown on Fig. 7.

There are significant problems with the carbonation of serpentine related to the costs. Serpentine is unreactive without a heat treatment. Olivine requires no heat treatment but is less common than serpentine. After heat treatment, serpentine reacts quickly, but the maximum conversion is lower than Olivine (Gerdemann et al., 2003). Wollastonita is another mineral that has a large capacity to uptake CO_2 and safety storage it. Much work is still need to understand these reactions and increase their carbonation rate, which is essentially the same as Olivine (Gerdemann et al., 2003).

Olivine and Wollastonite exhibit the best potential for capture and storage CO_2. The Mg-silicate olivine provided the basis for a process feasibility study, which determined a carbonation cost of $69 per ton of CO2 sequestered (O'Connor et al., 2004). However, Serpentine availability makes it the most interesting CO_2 sink, but it's being unsuccessful at activating the serpentine without a previous heat treatment. (O'Connor et al., 2004).

According to this, the resources and availability of the mineral capable of acting as an atmospheric CO2 sink is one of the main factors, so it is the energy costs that may make CCS impractical and the necessity of accelerating the kinetics of the carbonation reaction (Rigopoulos et al., 2015a, Rigopoulos et al., 2015b).

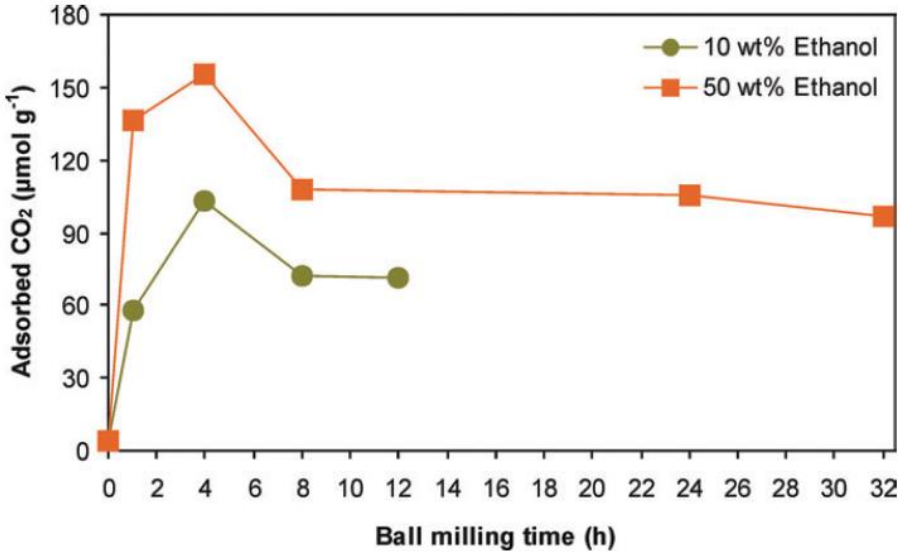

Fig. 8. Quantity of adsorbed CO_2 (µmol g^{-1}) versus ball milling time (h) for the starting material and representative nanomaterials produced after the addition of 10 and 50 wt% ethanol (Rigopoulos et al., 2015b).

The kinetics of the reaction can also be accelerated by decreasing the particle size. The long milling process improves the capacity of the minerals that has affinity to CO_2 to safety storage it (Rigopoulos et al., 2015a, Rigopoulos et al., 2015b). This is due to the increase of the specific surface area and pore volume is increase after the milling process. The pore volume is probably the most important parameter for the CO_2 storage in the milling processes (Rigopoulos et al., 2015a). In Olivine samples that has been ball milled for 4 hours, and saturated with 50% ethanol has reached an increase of 295% in the total CO_2 storage capacity compared to the reference un-milled sample (Rigopoulos et al., 2015a). The latter is due to the increase of the adsorption generated by the increase of pore volume and the use of ethanol instead of water in the wet ball milling process, which leads to the formation of smaller, rounded and uniform particles increasing their specific surface area.

It results in possibility to estimating an initial positive trend between ball milling time and CO_2 uptake, with a maximum carbonation rate at 4h of ball milling. Longer ball milling times tends to reduce the carbonation rate (Fig. 8) (Rigopoulos et al., 2015b). After only four hours the maximum an important increase of CO_2 uptake was observed. This method can become a promising preparation technique for development of piroxenitic nanomaterials for the safe ex-situ mineral carbonation (Rigopoulos et al., 2015b). It should be pointed out that the addition of 50wt% ethanol results in a greater mineral carbonation compared to the addition of 10wt% ethanol (Fig. 8) (Rigopoulos et al., 2015b).

In order to storage indefinitely and safety the CO_2 atmospheric, it is needed to increase the kinetics of the carbonation reaction of pre-heated serpentine. Much work is still needed to enhance the CO_2 uptake in the mineral carbonation technology referred to the serpentine, and understand its reaction in order to reduce their costs.

2. Objectives

Global warming is increasing each year due to the anthropogenic GHG emissions, especially of CO_2. Without additional efforts of those in place today the temperature at the end of this century will raise on a range of 3,7 ºC to 4,8ºC. In the Paris summit 2015 a global goal to limit global warming bellow 2ºC relative to pre-industrial global has been proposed. This goal can only be achieved with CDR technologies that are able to store safety and permanently the CO_2 having no risk of re-release on the atmosphere. That is where mineral carbonation storage technology CCS takes place, being able to trap CO_2 into stable carbonates minerals. But there is still much work needed in order to find a feasible way to make it happen.

The aim of this thesis is the feasibility study of the carbonation reaction of peridotites and serpentines with Mg-rich composition. These minerals have been proved to have higher affinity towards sinking of CO_2. The focus is on reproducing the experiments that gave the higher rate of carbonation with the lower energy required cost, published at Kelemen and Matter, 2008, with a variety of 6 non-pretreated samples (peridotites and serpentine). The samples where grounded to powder and exposed to 185ºC at 1 bar of CO_2 pressure for 2 hours (Gas-solid interaction).

The rate of carbonation and the kinetics of these reactions are estimated by calculating the area changes before and after carbonation of the main characteristic peaks of the X-Ray Powder Diffraction and FTIR Transmission resultant spectrums. Acid triggered de-carbonation experiment is used to estimate the carbonation rate of the different samples under this thesis conditions.

The behavior of the different samples will be analyzed in order to study the relation between each samples Mg# and Ca# composition with the carbonation formation. The affinity of the samples towards carbonation is defined as a feasible factor for carbonation formation. Therefore this thesis aims to analyze a feasible trend depending on the mineralogy and composition of different samples towards carbonation formation.

3. Samples Characterization

3.1. Samples Introduction

The samples used on this study were taken from Hisponiola, which is located at the North Edge of the Caribbean plate, where the Cretaceous Greater Antilles island arc system and the North American Plate collide (Marchesi et al., 2016; Escuder Viruete et al., 2010). It constitutes a NW-SW oriented belt of ultramafic rocks are mostly composed of serpentinized hazburgite with minor lherzolites, piroxenes and dunites (Lewis et al., 2006). Most of these ultramafic rocks were peridotites formed in the upper mantle which it has been uplifted and exposed to weathering. Therefore it partially –in some areas, fully - serpentinized the peridotites, and it conforms the main serpentine belt: the Loma Caribe peridotite which is about 4-5km wide and extends for 95km (Fig. 9) (Marchesi et al., 2016; Lewis et al., 2006).

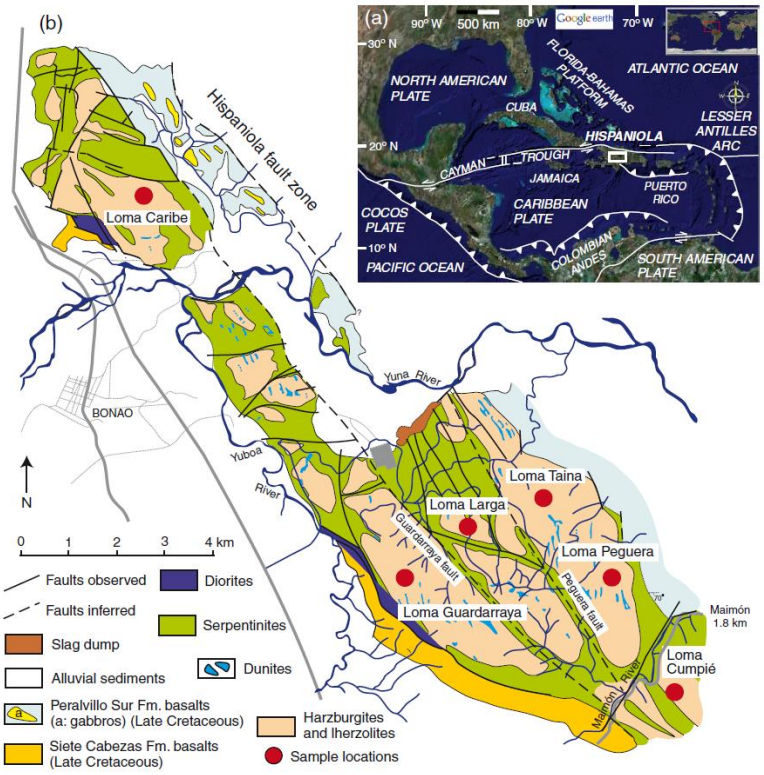

Fig. 9. (a) Geological provinces of the Caribbean region with location of modern plate boundaries and major tectonic elements. Modified from Draper et al., (1994) above an image from Google Earth, White box indicated the geographic location of the Loma Caribe peridotite in Central Hispaniola. (b) Geological Sketch map of the Loma Caribe peridotite with sample locations (red circles) (Marchesi et al., 2016).

The kinetics of the carbonations reaction is related to the mineral composition and to the mayor elements of the original peridotite. In order to find a feasible way to reproduce an ex-situ carbonation reaction is important to understand its behavior in different minerals and composition. For this study we selected 6 samples that represent the whole composition of the Loma Caribe complex (Fig. 9 and 10). The samples are already being characterized in Marchesi et al., 2016, which were giving to us with the collaboration of the Universitat de Barcleona

(UB). The selected samples are Dunite, Hazburgita, Clinopyroxene Hazburgite, Lherzolites and Serpentines (a fully serpentinized peridotite and an Antigorite). The Modal proportions and whole rock major element composition is found in the table 1.

Fig. 10. Original samples. (A) LT-1, Dunite; (B) LT-3, Hazburgite; (C) LT-4, Clinopyroxene Hazburgite; (D) C629-9, Lherzolite; (E) 14-SC-7, Serpentine (Mostly Lizardite); (F) 09-LV-IIA, Serpentine (Mostly Antigorite)

The peridotites are partially serpentinized with minor carbonates, and the interpretation of their whole-rock composition requires an evaluation of the potential interaction between rock and fluids at low temperatures. It is easy to appreciate its similarity with ophiolitic peridotes but with lower MgO/SiO_2 ratio (Fig. 11). This was caused by the dissolution of Brucite and serpentine or the SiO2 enrichment by reaction with fluids containing aqueous silica during serpentinization (Marchesi et al., 2016). Comparing the slope between the peridotite samples to the abyssal peridotite that is being taking as a reference ophiliolitic peridote, it is very similar, which means that the Al_2O_3/SiO_2 remain constant during the alteration process.

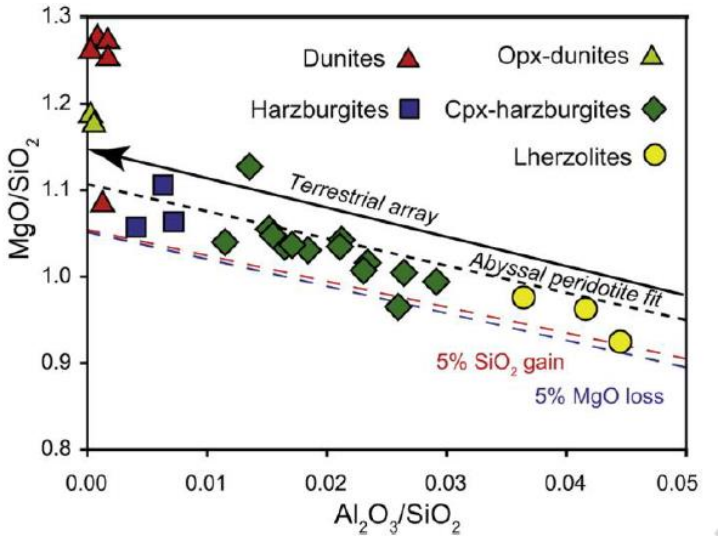

Fig. 11. Al_2O_3/SiO_2 vs MgO/SiO_2 in the Loma Caribe peridotes. Terrestrial array from Jagoutz et al. (1979) and Abyssal peridotite fit from Malvoisin (2015), (Marchesi et al., 2016).

The Modal proportions are shown in the table 1 (Marchesi et al., 2016). This was obtained as a geochemical interpretation of the whole rock geochemistry that estimates the idealised mineralogy of the samples. Therefore the altered samples will be characterized mainly by the Si addition and Mg losses.

As is it shown on the table 1, the Loss On Ignition (LOI) value are higher for the Dunite samples, and its value decreases with the presence of pyroxenes. The lower LOI value is found in the lherzolite, which is more resistant to serpentinization.

The serpentine samples are the product of the peridotite alteration. Both of the samples are partially carbonated. Therefore, its LOI values are expected to be very high. In the sample *14-SC-7* the lizardite is the most abundant mineral and forms a mesh texture, which is common in olivine serpentinization (ej: Garrido et al., 2006). Cr-spinel is partially oxidized to Ferrian chromite and Magnetite. In the sample 09-LV-IIA the most abundant mineral is the antigorite, forming an interpenetrating texture of Antigorite Blades.

Table 1. Modal proportions and Whole-rock major element compositions of Loma Caribe peridotites and its exact location (Marchesi et al., 2016), and selected serpentines with their mineral association with Mg # (Mg/(Mg+Fe)) and its equivalent in Ca (Ca/(Ca+Fe)). (*bdl = below detection level; ndl: not defined location*)

Lithology	**Dunite**	**Harzburgite**	**Cpx-harzburgite**	**Lherzolite**	**Serpentinite**	**Atg-serpentinite**
Sample	**LT-1**	**LT-3**	**LT-4**	**C629-9**	**14-SC-7**	**09-LV-IIA**
Location	Loma Taina	Loma Taina	Loma Taina	Loma Caribe		
Latitude (N)	18°55'8"	18°55'8"	18°55'8"	18°58'44"	*ndl*	*ndl*
Longitude (W)	70°19'18"	70°19'18"	70°19'18"	70°23'58"		
Mineral association (%)	Olivine (99) Spinel (1)	Olivine (76) Orthopyroxene (24)	Olivine (78) Orthopyroxene (19) Clinopyroxene (2) Spinel (1)	Olivine (66) Orthopyroxene (24) Clinopyroxene (8) Spinel (2)	Lizardite Chrysolite Cr-Spinel Magnetite	Antigorite Magnetite Dolomite Petlandite
SiO_2 (wt.%)	35.04	37.88	38.86	43.85	40.79	39.28
TiO_2	0.02	0.05	0.02	0.06	0.01	0.04
Al_2O_3	0.03	0.24	0.64	1.95	0.59	1.76
Fe_2O_3t	6.03	7.55	8.38	8.58	7.51	8.02
MnO	0.10	0.12	0.13	0.14	0.11	0.12
MgO	44.72	41.90	40.21	40.54	35.98	37.31
CaO	0.05	0.25	0.55	2.09	0.10	0.71
Na_2O	*bdl*	*bdl*	*bdl*	*bdl*	*Bdl*	*bdl*
K_2O	*bdl*	*bdl*	*bdl*	*bdl*	0.01	*bdl*
P_2O_5	0.01	0.01	0.01	0.01	0.00	0.01
LOI	13.71	11.65	10.57	1.94	14.10	12.16
Total	99.70	99.65	99.37	99.15	99.20	99.41
Mg #	0.864	0.826	0.805	0.802	0.804	0.800
Ca #	0.008	0.033	0.063	0.199	0.013	0.083

3.2. Samples Distribution

The samples were powdered until the grain size was suitable for doing the experiments and then weighted, as is it shown on table 2.

Table 2. Weight of the samples in grams that were ground to powder and separated them in different Eppendorf sample holders with their correspondent distinctive A,B and C.

Sample	LT-1	LT-3	LT-4	C629-9	14-SC-7	09-LV-II
A (g)	3.4	6.3	12.8	19.3	2.7	3.48
B (g)	2.5	7	4.5	22.8	2.9	2.7
C (g)	4	4.5	-	12.8	2.8	3.3

The samples are already being categorized using modal proportions and whole rock major element composition, but, in order to understand the carbonation and hydration reaction of peridotites and serpentines it is important to have a high qualitative mineral analysis before the experiment. The methods used are XRD, acid triggered de-carbonation and FTIR for every sample.

4. Experiment Procedure

4.1. X-Ray Powder Diffraction (XRD)

The vast majority of the minerals can be described as crystalline. The regular distribution between the spaces of the mineral components conforms a crystal network defined by the periodically repetition of the unit cell in form of parallelepiped. It contains all the information of the mineral crystal structure.

The crystal network is defined by reticular planes equally spaced in different orientations, represented by the Miller indices (h k l). The distance between each parallel hkl plane sequence is expressed as d_{hkl}. This distance determines the position of the diffraction peaks using the Bragg law which calculates the angle where constructive interference X-rays scattered by parallel planes of atoms, as follows:

$$\lambda=2d_{hkl}\sin\theta \qquad (11)$$

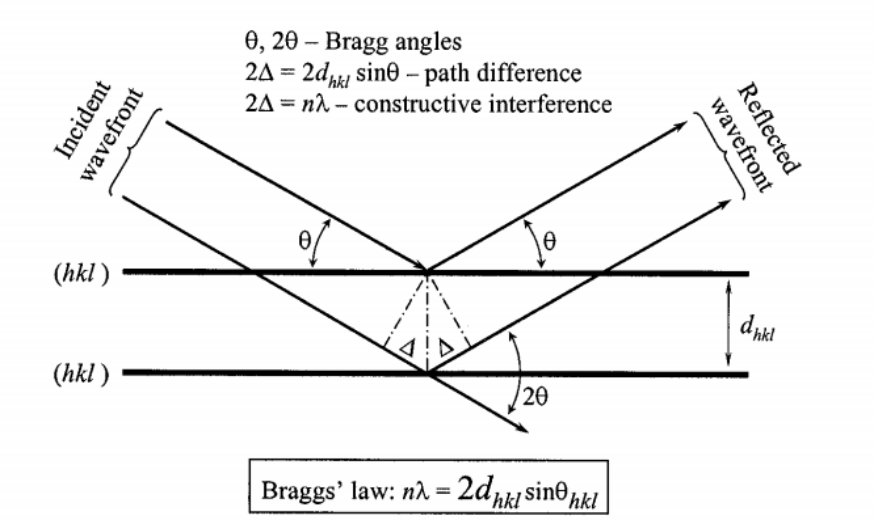

Fig. 12. Geometrical illustration of the Braggs' law (Pecharsky, V. and Zavalij, P., 2005)

Only a small fraction of crystals in the sample contributes to the measured diffraction peaks, due to the different orientations of the crystals that conforms the samples. Rotating the sample during the X-ray Diffraction increases the number of crystals that contribute to the measured diffraction peaks.

Each mineral has been characterized by the d_{hkl} values, which are stored on diverse databases, and by comparison of the measured diffraction peaks with the tabulated unique d-spacing of each mineral is possible to identify each mineral presented in the sample.

4.1.1. Preparation and conditions for the experiments

For our experiments we used the instrument Buker D8 Advanced, equipped with a theta-theta goniometer with a rotating sample holder, at the Center for Research in NanoEngineering (CRnE).

Fig. 13. Buker D8 Advanced at the Center for Research in NanoEngineering (CRnE)

The powder material was pressed manually by means of a glass plate to get a flat surface in a cylindrical sample holder.

The range of analysed angles goes from 1º to 60º using a step-size of 0.019747º and measuring time of 2 seconds per step. The Goniometer Radius used is 217.5º, Cu $K\alpha_1$ radiation (λ = 1.5406 Å), Work power: 40 kV – 40mA, using a Ge Monochrome and analysed by Lynxeye (1D).

4.2. Transmission Fourier Transform Infrared Spectroscopy (FTIR)

FTIR has proven to be a powerful tool for minerals characterization, which is based on the idea of interference of radiation between two beams to yield an interferogram, producing a signal as a function of the change of path-length between these two beams. By Fourier-transformation the domains of distance and frequency are interconvertible (Stuart, B. H., 2004), caused by the interaction between infrared radiations with matter. This interaction causes functional groups to uptake energy in form of vibration of the functional groups expressed as absorptions bands on the spectrum (Smidt, E., et al., 2011). Absorption can be easily converted on % transmittance.

The infrared radiation is passed through an interferometer to the sample, before reaching a detector where the signal is amplified. High frequency signals are eliminated by a filter. The data is converted and transferred to the computer for Fourier-transformation (Stuart, B. H., 2004).

The transmission spectroscopy is the oldest infrared method, in where is measured the absorption of infrared radiation at specific wavelengths as it passes through the sample.

For analyzing a solid sample exist different methods, the most common and used on this study is the use of alkali halide discs, in where the sample and the alkali halide (KBr is the most commonly used) are mixed and ground to powder with a mortar. The mix will be exposed to 5-10 tons of pressure to create a thin and flat pellet, which is transparent on the mid-infrared region. It is required around 2-3 mg of sample and 200mg of halide. If the crystal size of the sample is to large excessive scattering of radiation results, known as Christiansen effect (Stuart, B. H., 2004).

The infrared spectrum can be divided into three main regions: Far-infrared (<400 cm^{-1}), the Mid-infrared (4000-400 cm^{-1}) and the Near-infrared (13000-4000 cm^{-1})

4.2.1. Preparation and conditions for the experiments

Each small fraction of the sample, mixed with their correspondent KBr was pressed into pellets at 5 Tons of pressure for five minutes, with the hydraulic press SPECAC 15, and then analysed by FTIR Transmission. Sample should be thin and flat in order to avoid absorption band saturation.

The instrument used is FTIR Nicolet 6700 at the CRnE. The analysed spectra range goes form 225 cm^{-1} to 4000 cm^{-1}, using 64 scans at 1 resolution. The data Spacing is: 0482 cm^{-1}.

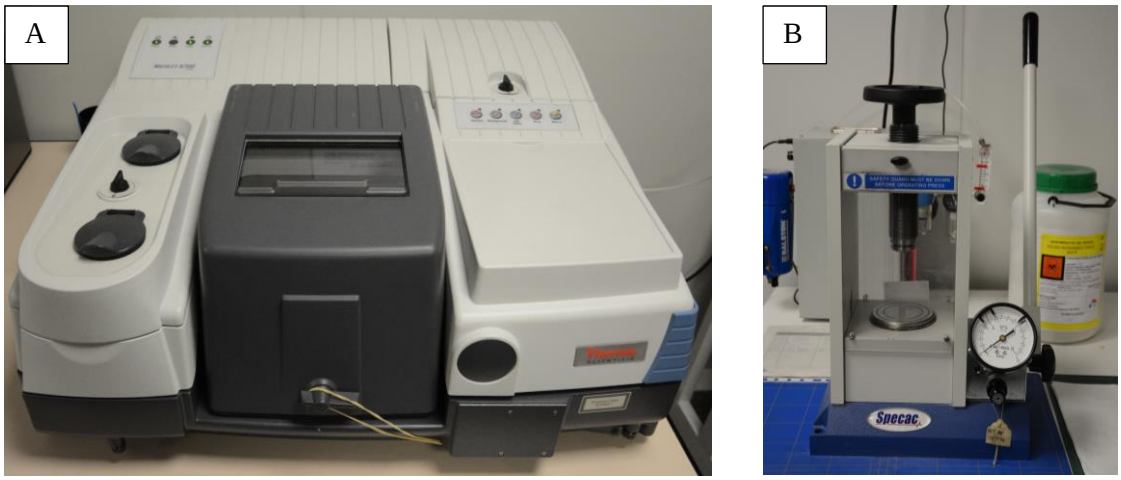

Fig. 14. (A) Transmission FTIR Nicolet 6700 at the CRnE. (B) Hydraulic press SPECAC 15 at the CRnE.

The data is collected with the program: Ominic. Before analysing every sample, the background spectrum was taken and extracted from each sample spectrum.

4.3. Acid Triggered de-Carbonation

Carbonate minerals are unstable in contact with hydrochloric acid, and react exothermically to form CO_2, H_2O, dissolved Calcium/Magnesium/Iron/and others (Ca^{2+}, Mg^{2+}, Fe^{2+}, …) and dissolved chlorine (Cl^-).

$$(\mathrm{Ca} \,/\, \mathrm{Fe} \,/\, \mathrm{Mg})\,\mathrm{CO_3} + \mathrm{2HCl} \rightarrow \mathrm{CO_2} + \mathrm{Ca^{2+}}, \mathrm{Mg^{2+}}, \mathrm{Fe^{2+}} + 2Cl^- + H_2O \qquad (12)$$

After leaving the samples for 24 hours with exceeding HCl in a closed glass sample holder, the whole carbonate will react and the CO_2 product should separate from the sample. After the reaction, it is possible to compute the quantity of carbonate presented on the original sample by comparing the weights before and after CO_2 liberation.

4.4. Carbonation Experiment Procedure

Each sample will be exposed to 1 bar of CO_2 and atmospheric pressure at 185º degrees using a reactor.

The sample will be placed inside a cylindrical reactor in where both extremes will be blocked by glasswhool which keeps the sample thermically insolated in the reactor but allows gas to flux inside it. The sample and the reactor were weighted as it shows on table 3. The reactor will be placed on a temperature chamber, where it is possible to have a very accurate control of the reaction temperature. Once it is placed, the gas entry is connected to the reactor. The gas exit from the reactor is connected to a manual pressuring system.

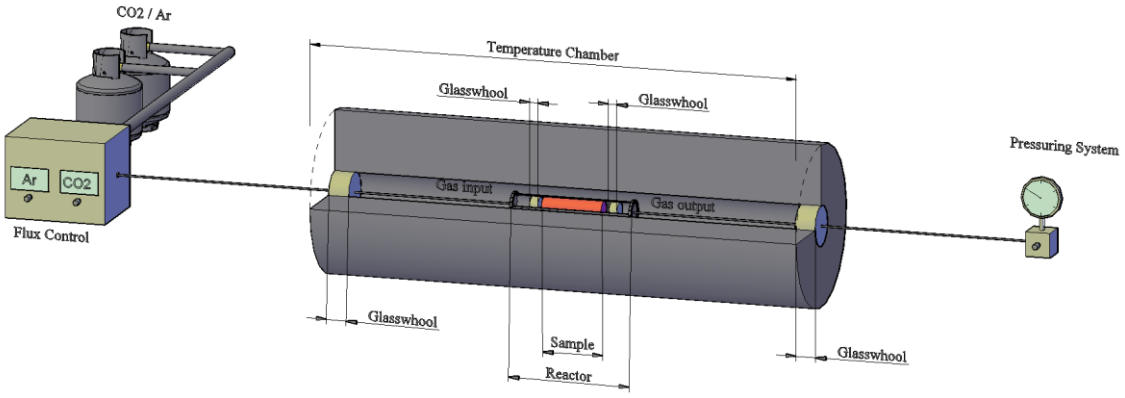

Fig. 15. Schematic of the Reactor, where the carbonation experiment took place.

In order to achieve the ideal conditions for the experiment, the temperature was raised at a constant rate of 5 degrees per minute, injecting argon with a constant flux of 20ml/min, until achieving 185 degrees. Once it reaches the desired temperature the argon injection is cut off and CO_2 injection starts with a flux of 24.7 ml/min. The pressure of CO_2 was raised to 1 atm with the manual pressuring system.

Table 3. Weights of the samples before and after the reaction

Sample	Sample before reaction(g)	Sample after reaction(g)	Sample with the Reactor after Reaction (g)	Sample with the Reactor before Reaction (g)
LT-1/B/1	2.4541	2.248	68.283	68.556
LT-3/B/1	2.55	2.248	68.293	68.704
LT-4/B/1	2.6722	2.584	68.794	68.869
C626-9/B/1	2.6651	2.617	69.282	69.321
14-SC-7/B/1	2.4442	2.043	68.125	68.508
09-LV-IIA/B/1	2.6420	2.481	68.683	69.492

The mass losses can be attributed to human factor and the sample that got stock on the glasswhool.

5. Samples Characterization

5.1. XRD Interpretation

Generally, the samples are partially altered, raising the base line and generating wide peaks with less definition (showing a Gauss bell model). The area form 1º to 10º has been cut off from interpretation. The results are shown on the Fig. A1 and Fig. A2.

For the interpretation we used the RRUFF Database as a reference (Lafuente B., et al., 2015), comparing the following minerals with its correspondent RRUFF Reference: (Fosterite: R040018; Lizardite: R060006; Antigorite: R070228; Enstatite: R040093; Diopside: R040009; Calcite: R040070; Magnesite: R040114; Dolomite: R040030).

The peridotites samples have a similar XRD spectrum reflecting similar phase minerals, but the proportions are different in each sample. The Olivine's peaks have negative correlation with the Serpentines's peaks (as it is usually seen on other studies ej: Lafay R., et al., 2014; Lafay R. , et al., 2012; Bishop, J., et al., 2013) and minor negative correlation with carbonate's peaks, where the olivine is being serpentinized and carbonated. The spectrum of sample 14-SC-7/A is also similar to the peridotites samples, reflecting an Olivine that is almost fully serpentinized and partially carbonated.

The peak of the serpentines also has a correlation with the LOI value of each sample, at lower LOI values, the less serpentine proportion there is. The sample C-629-9/C, whit a LOI value of 1.94 have the lower serpentine's proportion, comparing it to the Olivine's peaks.

Carbonates are present in all the samples. Calcite is also detected in each of the samples and Dolomite is present in almost all of them. Magnesite is detectable in the sample LT-1/C, which has the highest Mg#.

Brucite appears in the peridotite samples, mainly in the sample LT-1/C who has the bigger Mg#. This mineral proportion tends to fade out at little changes on the Mg#.

The sample 09-LV-II/B is the one that most differs from the other samples. The main present mineral phase is the Serpentine. Its 100 peak counts have one magnitude higher than the other samples, reaching intensity of 1.32E+05, differing form the sample 14-SC-7/A that reaches until 1.01E+04 on its 100 peak count. There is also difference on the 2-Theta angle of the 100 peak for serpentine comparing it to the one presented on the other samples.

5.2. FTIR Transmission interpretation

A small fraction of each powder sample is mixed with Potasium Bromide (KBr) (Table 4) and weighted with an analytical balance.

Table 4. Weights of the powder samples taken and the KBr in order to create the tablets for IR analysis.

	LT-1 (B)	LT-3 (B)	LT-4 (A)	C629-9 (B)	14-SC-7 (B)	09-LV-IIA (A)
Sample (g)	0.0004	0.0004	0.0004	0.0004	0.00039	0.0004
KBr (g)	0.2506	0.2507	0.2508	0.2502	0.25085	0.2509

For the interpretation we used the same Reference Database as for XRD (Lafuente B., et al., 2015). In this case, rather than look for specific mineral phases, we are going to look for absorptions of resonant frequencies of the bonds or groups of molecules.

The values of the peak absorptions are determined by the molecular potential energy surfaces and the bonds that interact in that molecule at different Mg#, the absorption peaks differ between a range of values (ej: Hamilton, V., 2000).

All the samples shows absorptions of carbonates in 1538-13520cm^{-1} (ej: Turianicová, E., et al., 2013; Nichols, A., and Wysoczanski, R., 2007; Neubeck, A., 2015; Coates, J., 2000; Smidt, E., et al., 2011, Böttcher, M. and Gehlken, P., 1995, Reig, F., et al., 2002, Bruckman, V. and Wriessnig, K., 2013) with a resemblance on the main peaks absorption on the 1419 to 1468 almost in every sample, generating a characteristic doublet of the asymemetric C-O stretching mode of magnesite (Turianicová, E., et al., 2013, Nichols, A., and Wysoczanski, R., 2007; Zhang, Z., et al., 2006). The magnesium carbonate reflect a complexity nature in form of large number of possible phases with strong kinetic inhibitions that depends on temperature, parital pressure of CO_2 and other parameters (Turianicová, E., et al., 2013; Hänchen, M., et al., 2007).

The band at 1384 cm^{-1} in every sample is characteristic of the NO_3^- absorption band (Smidt, E., et al., 2011; Zhang, Z., et al., 2006). Water is present in OH^- stretching bands between 3490-3280 cm^{-1} and 1625 cm^{-1} (ej: Neubeck, A., 2015).

The main typical absorption band for Silicate ion is 1100-900 cm^{-1} (Coates, J., 2000) in form of Si-O asymmetric vibration (Saikia, B. et al., 2009). At low frequencies the form of energy are stretching and bending modes (Neubeck, A., 2015).

Serpentine is also present in all the samples, and its absorption peaks are clear and constant for almost every single representative peak. As is it shown in Mellini, M., et al., 2002 and Trittshack, R., 2012, it is possible to infer that the serpentine's mineral that is product of the hydration reaction of the peridotites is Lizardite in this study, and it can be distinguish from Antigorite which is the main mineral phase on the sample 09-LV-II/A. Even though they have very similar main peak absorption, as it is expected, there are critical absorptions that can be interpreted as a different mineral phases (Fig. B5, Fig B6).

The rate of serpentinization can be determined by the ratio of the characteristic band of the hydroxyl group (OH^-) in serpentines-brucite and the Si-O group in peridotites, by using integrated band intensities. This gives two calibration curves that can be used to determine

serpentinization reaction kinetics (Lafay, R., et al., 2012), and so it works for carbonation reactions.

Table 5. FTIR peak positions from 225 to 4000 cm^{-1} of the minerals that are present in the sample. The observed peak positions are compared with the reference Database on this study (Lafuente B., et al., 2015), and different studies with similar samples (ej: Neubeck, A., 2015; ej: Lafay R., et al., 2014; Lafay R. , et al., 2012; Golightly, J. and Arancibia, O., 1979; Saikia, B. et al., 2009; Mellini, M., et al., 2002; Trittshack, R., 2012; Hamilton, V., 2000, Omori, K. (1971))

Mineral	LT-1/B	LT-3/B	LT-4/A	C626-9/B	14-SC-7/B	09-LV-II/A
Mg/(Mg+Fe)	0.864	0.826	0.805	0.802	0.804	0.8
Olivine	1050	1052	1050	1056	1047	-
	968.1	965.7	972	981.6 - 1009	-	-
	882.3	-	886.1	882.3	-	-
	838.4	839.4	837.9	838.9	-	-
	612.3	613.7	614.7	608.9 - 613	-	-
	560.7	562.2	565	551.6	561.7	-
	459.5	459.9	461.4	465.7	463.3	-
Orthopyroxene	-	1170	-	-	-	-
	-	-	1130	1129	-	-
	-	965.7	972	981.6 - 1009	-	-
	-	-	886.1	-	-	-
	-	-	-	551.6	-	-
	-	450.8	453.7	457.1	-	-
Clinopyroxene	-	-	972	981.6 - 1009	-	-
	-	-	500.4	504.3	-	-
	-	-	-	443.6	-	-
Serpentine	3690	3687	3688	3687	3690	3678
	3646	3649	3648	3643	3648	3616
	1079	1076	1075	1047-1067	1082	1081
	968.1	965.7	972	981.6 - 1009	960.4	981.1
	-	-	-	-	-	638.3
	612.3	613.7	614.7	608.9 - 613.3	611.3	619
	-	-	-	-	-	567
	445	443.6	445	446.9	445	446.4
Carbonates	1455	1468	1456	1469	-	1451
	-	1419	1419	1420	1422	-
	1369-1488	1360-1501	1352-1514	1369-1488	1362-1477	1363-1539
N-H	1384	1384	1384	1384	1384	1384

The absorption bands from 800-1150 cm^{-1} and 400-700cm^{-1} indicates the presence of silicates. The comparison with the absorption bands of the Fosterite on Saikia, B. et al., 2009, and Duke, D., et al., 1964 reveals the presence of Olivine (Fig. B1 – B4), and in some samples Orthopiroxene as Estatite.

Orthopyroxene are difficult to distinguish from Clinopyroxene and olivine, due to the very similar critical absorption bands and peaks, but they can be distinguished from each other (ej: Hamilton, V., 2000). Taking into detail the absorption bands from silicates in the samples LT-3/B, LT-4/A and C-626-9/B, it is possible to distinguish critical absorption peaks similar to those of the Enstatie and Diopside on Hamilton, V., 2000 and Saikia, B. et al., 2009. Orthopyroxene has critical peaks on the absorption band at 600-400 cm^{-1} generating an overall V-Shaped appearance (LT-3 Fig. B2, LT-4 Fig. B3) (Hamilton, V., 2000), therefore it is possible to recognize the presence of Orthopyroxene is this specific samples. Same ways comparing this absorption bands to those of the Diopside on Hamilton, V., 2000 and Omori, K. (1971), there are similarities on the main peak absorptions, and in the band 600-400 cm^{-1} lack the V shape of the orthopyroxenes (LT-4 Fig, B3, C-626-9 Fig. B4) (Hamilton, V., 2000), therefore it is possible to distinguish the presence of Clinopyroxenes in these samples, as it can be seen on the table 5 and Fig B2 - B4.

6. Carbonation Reaction Results

All the samples are analyzed before and after carbonation with XRD, Transmission FTIR and acid triggered de-carbonation, in order to understand the carbonation reaction that has taken place on the reactor.

6.1. Acid Triggered de-Carbonation

All the samples before and after carbonation were mixed with exceeding HCl to make sure that all the carbonates will react. The correspondent weights are shown in the table 6. During the reaction all samples effervesced and got heated up, demonstrating the presence of carbonates and its exothermic reaction with HCl.

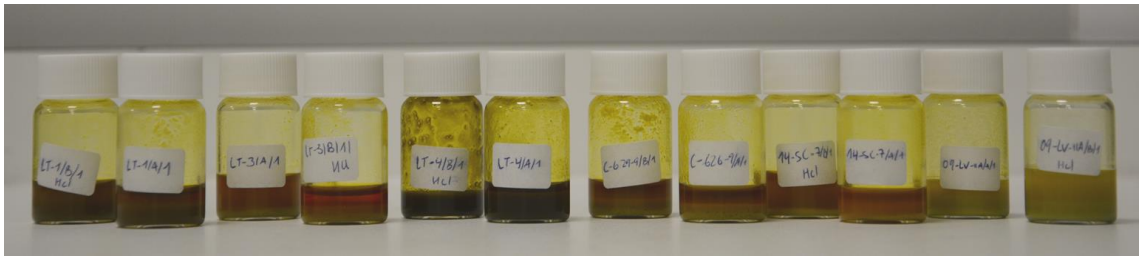

Fig. 16. Sample before and after carbonation reacting with exceeding HCl

The serpentine samples has the bigger CO_2 mass loss comparing it to the peridotites samples, and a steeper difference between the before and after carbonation. The sample 09-LV-IIA has a very high value of % mass loss due to CO_2 liberating after the acid triggered de-carbonation comparing it to the other samples, especially for the samples after the carbonation reaction. The sample 14-SC-7 also presents a similar behavior.

Table 6. Weights of the samples (before and after carbonation) before and after acid triggered de-carbonation with HCl.

Sample	Samples weight (g)	Hcl (g)	Package+Sample+Hcl After Reaction (g)	CO2 liberating (g)	Mass Loss (g)	Mass Loss %	Difference After/Before carbonation %
LT-1/B/1	0.7757	15.316	16.0909	16.0671	0.0246	3.171329	2.705185844
LT-1/A/1	0.8152	14.972	15.7973	15.7832	0.0038	0.466143	
LT-3/B/1	0.8026	14.65	15.453	15.4386	0.0141	1.75679	0.54868443
LT-3/A/1	0.7698	15.714	16.4842	16.4749	0.0093	1.208106	
LT-4/B/1	0.8086	13.722	14.5289	14.5277	0.0029	0.358645	-0.610781231
LT-4/A/1	0.8046	14.871	15.676	15.668	0.0078	0.969426	
C626-9/B/1	0.8495	14.795	15.6448	15.6295	0.0152	1.789288	1.238389613
C626-9/A/1	0.835	14.608	15.4434	15.4387	0.0046	0.550898	
14-SC-7/B/1	0.7632	15.919	16.6823	16.6574	0.0246	3.22327	2.814892097
14-SC-7/A/1	0.7591	14.304	15.0633	15.0599	0.0031	0.408378	
09-LV-IIA/B/1	0.7755	16.437	17.2111	17.1693	0.043	5.54481	3.925165077
09-LV-IIA/A/1	0.7656	14.679	15.4446	15.4318	0.0124	1.619645	

Out of the peridotites samples, the sample LT-1 has clearly carbonated more than the others, showing a big difference between the %mass loss before and after carbonation, followed by C-626-9. On the other hand, the sample LT-3 has similar % mass loss comparing it to the C-626-9 after carbonation, but before carbonation it has a very high % mass loss, which lowers the carbonation rate considerably.

The sample LT-4 present a non-logical pattern, in where there is bigger mass losses on the before carbonated sample comparing it to the carbonated sample, which can be attributed to human factor.

6.2. X-Ray Powder Diffraction

The range of analyzed angles goes from 10º to 40º targeting mainly the 100 peaks for Carbonates, Serpentine and Silicates. The results for every sample before and after carbonation are shown in Fig. A3 until Fig. A8.

The analysis results show that the spectrums from the same samples before and after carbonation are almost equal, but they show little differences that reflect the reactions occurred on the reactor.

The peridotites samples have a clear baseline with little noise. On the other hand, serpentines samples present a spectrum with sharp 100 peaks, but its baseline have a lot of noise, which makes it difficult to recognize little mineral proportions (Fig 17), and harder for detecting very little variations.

The spectrums for all the samples have very similar count number for baseline and peaks, reflecting optimal conditions on the experimental part. By defining peak areas and/or intensities (counts), it is possible to compare the difference between the spectrums before and after carbonation.

Magnesite is only recognizable in the sample LT-1. Calcite is present in all the samples before and after carbonation with little variations with both correspondent spectrums, similar to the Dolomite peaks, but in this case, it is not present in all the samples. It is not possible to distinguish an increment of magnesite, which is the main mineral formation in carbonation of peridotites and serpentines (i.e. Lafay, R. et al, 2014, Lafay, R. et al, 2012, Turianicová, E., et al., 2013, Hänchen, M., et al., 2008, Sissmann, O., et al., 2014, Gadikota, G., et al, 2014, Santos., R., et al., 2015, Bruckman, V., and Wriessnig, K., 2013).

Overall, the 100 peak for Calcite has increased for every peridotite sample, which is not the case for serpentines samples. Dolomite present arbitrary variations with non-recognizable pattern.

The Olivine peaks also present variations before and after the carbonation reaction. Again this variation does not follow a recognizable pattern.

The clinopiroxenes and orthopyroxenes in the samples remain constant before and after carbonation for all the samples. If there are any changes on these mineral components, it will be very small variation which cannot be detectable with this method.

The spectrum of the sample 09-LV-IIA has a very sharp peaks for Antigorite with very high intensities. It counts for the 100 peak reach until 8.823E+04 counts after carbonation and 1.322E+05 counts (which coincide with the first XRD analysis for characterization) before carbonation, which is one higher magnitude order comparing it to all the other samples. For the other serpentine sample (14-SC-7), the count value before and after carbonation of the 100 peak for Lizardite are: 1.007E+04 (Also coincide with the first XRD analysis for characterization) and 9.768E+03 correspondently.

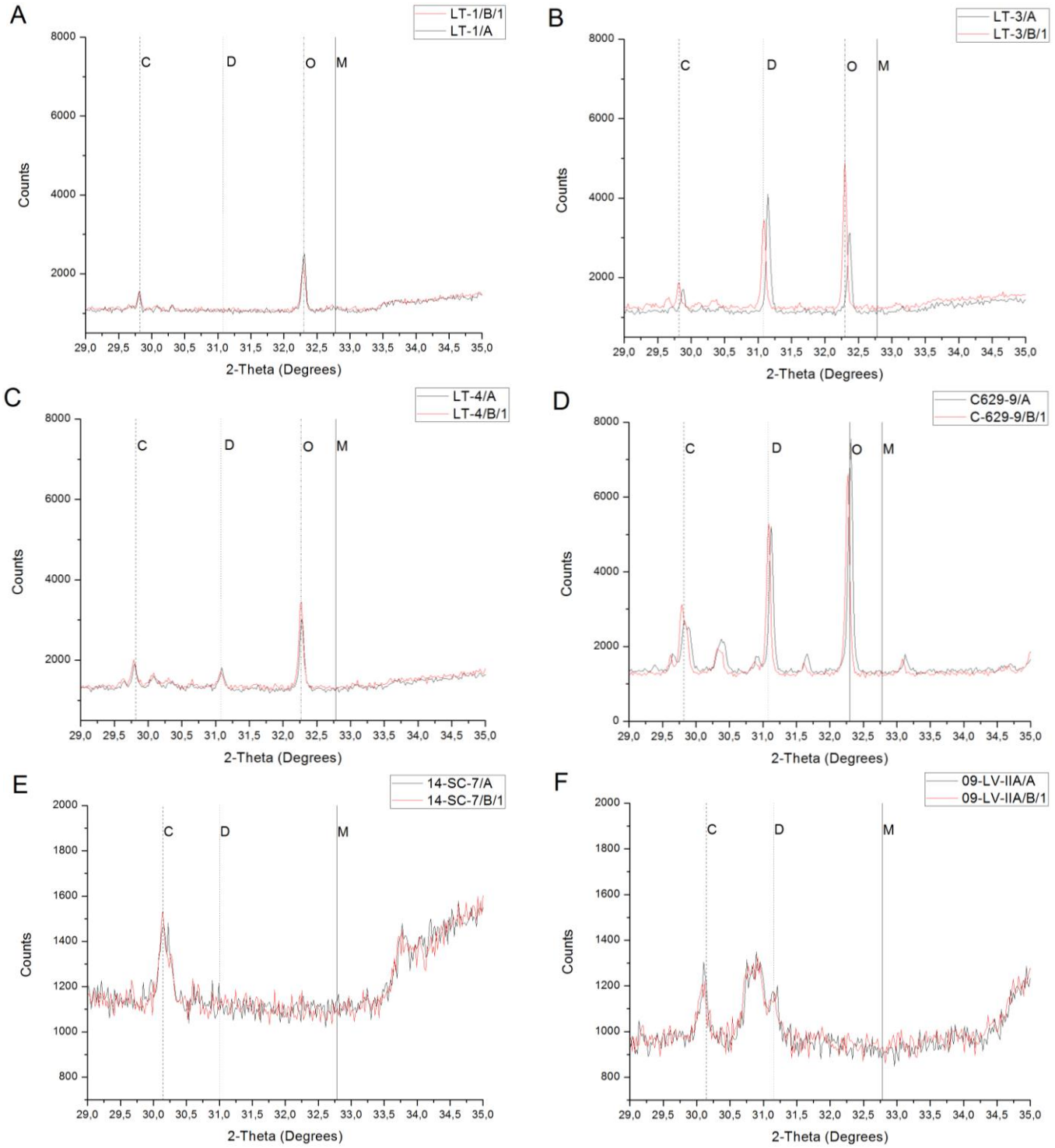

Fig. 17. X-Ray Powder Diffraction spectrum results before and after carbonation for every sample superposed, focused on the area of 100 peak characteristic of carbonates. (A) LT-1, (B) LT-3, (C) LT-4, (D) C-626-9, (E) 14-SC-7, (F) 09-LV-IIA.

The serpentine peak varies in every sample. For the serpentine samples the peak intensity after carbonation is lower than before carbonation. On the other hand, the peak counts for serpentine in the peridotite samples are higher after carbonation than before carbonation, excluding the sample C-626-9, which is the one who has more Olivine proportion and the one who has the

lower LOI value. This explains why this sample has the greater resistance towards serpetinization.

These results reveal the direct relation of the LOI values with serpentinization in the peridotite samples. Serpentine samples have an inverse behaviour regarding LOI values, even though they both have a high LOI value, they serpentine proportion after carbonation is lower.

Overall, the XRD results revealed that the main minerals that has been involved on the carbonation reaction is the Olivine, Serpentine, Calcite and Dolomite. Other mineral variation are so small that cannot be recognizable due to the background noise (i.e: Magnesite) or its variation is lower than the detectable limitation of the method.

6.3. Transmission FTIR

The FTIR spectrums are very sensible to the amount of sample taken (Stuart, B. H., 2004), and even though the samples were weighted with an analytical weight balance, the spectrum shows little variation between the sample taken for the spectrums before and after carbonation for each sample. The results of the transmission FTIR analysis of every sample before and after carbonation are shown in Fig. B1 until B6.

In all samples it is possible to recognize the double characteristic peak of the magnesite (ej: Turianicová, E., et al., 2013, Nichols, A., and Wysoczanski, R., 2007; Zhang, Z., et al., 2006).

Table 7. FTIR peak positions from 225 to 4000 cm^{-1} of the minerals of the samples after carbonation. The observed peak positions are compared with the reference Database on this study (Lafuente B., et al., 2015), and different studies with similar samples (ej: Neubeck, A., 2015; ej: Lafay R., et al., 2014; Lafay R. , et al., 2012; Golightly, J. and Arancibia, O., 1979; Saikia, B. et al., 2009; Mellini, M., et al., 2002; Trittshack, R., 2012; Hamilton, V., 2000, Omori, K. 1971, Coates, J., 2000; Smidt, E., et al., 2011)

Mineral	LT-1/B	LT-3/B	LT-4/A	C626-9/B	14-SC-7/B	09-LV-II/A
Mg/(Mg+Fe)	0.864	0.826	0.805	0.802	0.804	0.8
Olivine	1051	1047	1050	1059	1044	-
	967.6	967.1	972.9	998.5-982.1	-	-
	-	-	886.1	885.2	-	-
	-	-	839.9	838.9	-	-
	612.8	616.6	615.7	612.8-609.4	-	-
	559,3	561.7	562.2	545.3	565	-
	462.8	463.3	461.4	462.4	462.8	-
Orthopyroxene	-	1163	-	-	-	-
	-	-	-	1129	-	-
	-	967.1	972.9	998.5-982.1	-	-
	-	-	886.6	-	-	-
	-	-	-	545.3	-	-
	-	459.5	457.1	453.2	-	-
Clinopyroxene	-	-	972.9	998.5-982.1	-	-
	-	-	500	503.3	-	-
	-	-	-	416.1	-	-
Serpentine	3688	3686	3688	3686	3688	3688
	3646	3652	3649	3647	3649	3649
	1075	1074	1079	1067-1047	1080	1079
	967.6	967.1	972.9	998.5-982.1	958.5	971.5
	612.8	616.6	615.7	612.8-609.4	640.9	615.7
	-	-	-	-	-	562.2
	446	448.4	445	442.6	443.6	447.4
Carbonates	1457	1466	1457	1456	1457	1457
	1419	1420	1437	1419	1419	149
	1358-1486	1362-1480	1360-1538	1369-1488	1349-1495	1363-1539
C=O	1727	1740	1740	1734	1735	1735
N-H	1384	1384	1384	1384	1384	1384

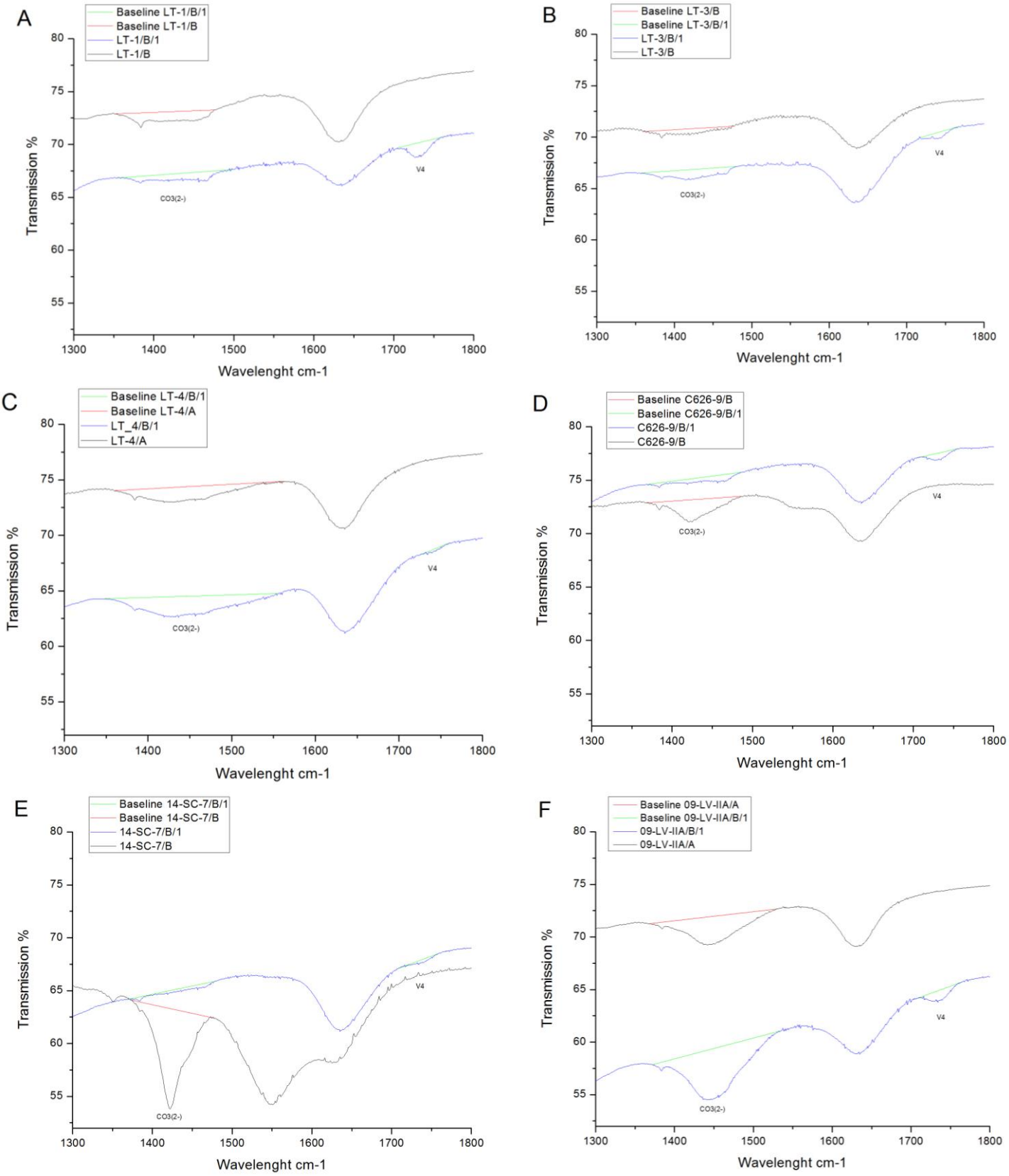

Fig. 18. FTIR Transmission spectrum result focused on the carbonated absorption band and main changes between the samples before carbonated, with their correspondent base line which will be used to compare the area changes between both spectrums for each sample. (A) LT-1, (B) LT-3, (C) LT-4, (D) C626-9-, (E) 14-SC-7, (F) 09-LV-IIA.

The analysis results show that after the carbonation all the samples exhibits absorption on the characteristic absorption band for C=O (Coates, J., 2000; Smidt, E., et al., 2011), which is located between 1740-1700 cm^{-1}, with resemblance on the peak at 1735 cm^{-1}. Comparing it to the reference database used in the study Lafuente B., et al., 2015 and Turianicová, E., et al., 2013, Bruckman, V. and Wriessnig, K., 2013, this peak coincide with a minor peak present in all carbonates (especially for Calcite). The area of this absorption band is a product of an increment of carbonates in the samples after carbonation. (Fig. 18)

The main peaks remain almost constant from the samples before and after carbonation, in where the carbonate absorption band and the V_4 stretching bands present the major changes (Table 7, Fig. 18). The carbonated absorption band area of the carbonated samples does not have an important increase comparing it to its correspondent non-carbonated sample.

The absorption bands for serpentines which are determined by the characteristic band of the hydroxyl group (-OH), have not a clear difference in any of the spectrums for each sample before and after carbonation. The serpentinization rate cannot be estimated by this method under this thesis set up conditions.

The absorption band at 1384 cm^{-1}, which characteristic of the NO_3^- absorption band (Smidt, E., et al., 2011; Zhang, Z., et al., 2006), remain constant for every sample before and after carbonation. Water is present in OH stretching bands, with a resemblance for every sample before and after carbonation in 1635 cm^{-1} (ej: Neubeck, A., 2015).

The main typical absorptions bands for Silicates remain constant for every peridotite samples before and after carbonation, which can be used as reference to compare the resultant spectrums by area peak normalization.

7. Discussion

All the results of the different methods express changes in the samples before and after carbonation, which reveals that the reaction took place in the reactor at the specific conditions of this study, based on Kelemen and Matter, 2008. There were not big mineral variation as in other studies (i.e.Lafay, R. et al, 2014, Lafay, R. et al, 2012, Turianicová, E., et al., 2013, Sissmann, O., et al., 2014, Gadikota, G., et al, 2014, Buckman, V., and Wriessnig, K., 2013), because there was no pre-treatment of the samples and they were exposed to a gas-solid interaction for 2 hours without any catalyst presence.

7.1. Acid Triggered de-Carbonation

Almost all the samples did have more % mass loss, once CO_2 was liberated of the reaction sample holder (Table. 6). The maximum value of carbonation reaction rate is lower than 4% for the serpentine sample 14-SC-7. This result reveals the maximum carbonation rates expected under this thesis set up conditions should be lower than 4%.

Comparing the mass loss of the samples after carbonation with their correspondent Mg# and Ca#, we found that the % mass loss values for the samples 09-LV-IIA and LT-4 has small resemblance with all the other samples, where the % mass loss is either too big or too small. LT-4 does not have a logical result (attributed to human factor), as it can be seen on (Fig.19). 09-LV-IIA has an exceeding % mass loss, probably because the carbonates that was already in the sample.

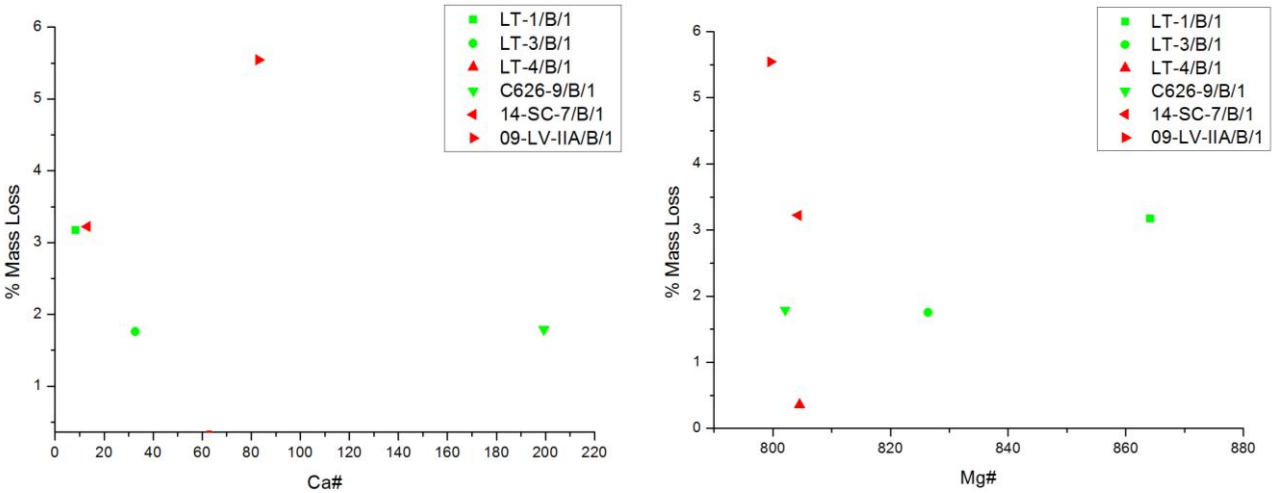

Fig. 19. Comparison between the mass loss % of the samples and the (Left) Ca# with a three-parameter logarithm function (Log3P1) and (Right) Mg# with a two-parameter logarithm function (Log2P2). The non-linear curves were calculated with OriginLab 8. Green: Peridotites samples, Red: Serpentines samples.

Excluding the result of the serpentine samples, because they have a complex behaviour towards carbonation reaction, and the LT-4, due to its non-logical result, it is possible to calculate a non-linear curve fit function in order to find a general carbonation trend curve. The results show an inverse relation between Mg# and Ca#. At higher Mg# the bigger the mass loss %, and at higher Ca#, the lower the mass loss. There is still a lot of work to do regarding the influence of Mg# and Ca# as a factor for carbonation of peridotites and serpentines.

7.2. X-Ray Powder Diffraction

This method result tremendously precise at mineral proportion greater than 5%. As it was discussed on acid triggered de-carbonation experiment, the maximum expected carbonation rate should be lower than 4%. This fact should be taken into account for a correct result interpretation.

The 100 peak for Magnesite does not seem to change after carbonation in any sample. It should be taking into account that the initial XRD characterization (Fig. A1, Fig. A2) shows a minimal mineral Magnesite proportion only in the LT-1 sample, and the maximum carbonation rate should be lower than 4%. Magnesite formation cannot be determined by using XRD under this thesis set up conditions (Fig. 17).

The serpentine 100 peaks on the serpentine samples have lower counts on the samples exposed to carbonation conditions. In the case for peridotites, the serpentine formation rate depends on the original LOI value (Table 8). This fact explains the behaviour of the sample C626-9, which has greater counts of the 100 peak for serpentines after the carbonation. Additionally, this sample has bigger olivine proportion compared to the other peridotites samples.

The sample LT-3 has important differences on the baseline for both correspondent spectrums (Fig. 17). In order to have a correct interpretation it should be taking into consideration the maximum carbonation rate expected should be lower than 4% and the LT-3 spectrum baseline differences. Under these conditions, both LT-3 resultant spectrums cannot be compared in a quantitative way using XRD. The sample C626-9 also differs on the baseline before and after carbonation, but this difference is not as significant as the one present on LT-3 sample (Fig. 17).

The spectrums of serpentine samples have noise in their correspondent baseline (Fig. 17). Under this conditions where the expected carbonation rate should be lower than 4%, a quantitative identification of carbonation formation cannot be conclusive for serpentines by using XRD.

Table 8. Counts of the 100 peaks for the minerals that have recognizable changes after the carbonation reaction and its correspondent LOI value (Marchesi et al., 2016).of the samples before the experiment.

	Original	100 Peaks Counts			
Sample	**LOI**	**Calcite**	**Dolomite**	**Olivine**	**serpentine**
LT-1/B/1		1558	-	2745	1.12E+04
LT-1/A	13.71	1538	-	2573	1.09E+04
Difference		20		172	260
LT-3/B/1		1868	3453	2652	1.45E+04
LT-3/A	11.65	1703	4106	2668	1.16E+04
Difference		165	-653	-16	2870
LT-4/B/1		2020	1703	3363	5664
LT-4/A	10.57	1907	1818	3229	5453
Difference		113	-115	134	211
C-626-9/B/1		3129	5290	5742	3055
C-626-9/A	1.94	2699	5208	5577	3277
Difference		430	82	165	-222
14-SC-7/B/1		1532	-	-	9768
14-SC-7/A	14.1	1470	-	-	1.01E+04
Difference		62	-	-	-302
09-LV-IIA/B/1		1222	1172	-	8.82E+04
09-LV-IIA/A	12.16	1304	1201	-	1.32E+05
Difference		-82	-29	-	-43970

Calcite increased in all the peridotite samples. This detected positive variation does not follow a recognizable trend as it was expected because the non-equal baseline of the samples and the maximum carbonation rate expected. Under this set up conditions it is possible to conclude that there is an increase of Calcite mineral proportion for all the peridotites samples. The serpentine samples do not have a conclusive result towards Calcite formation.

Dolomite also presents changes after carbonation. As it was expressed for Calcite, it does not follow a recognizable trend, but it can be concluded that this mineral has been involved in the carbonation reaction.

Olivine increased their counts on the 100 peak for almost every peridotite sample, excluding the sample LT-3 which presents a lower intensity. This can be attributed to the differences of the LT-3 spectrums baseline. Overall, the Olivine mineral seems to increase its mineral proportion after the carbonation reaction.

Is not possible to quantify the changes of the samples after carbonation by using XRD under this thesis set up conditions. Nevertheless it reveals mineralogical changes. Calcite did formed in all the peridotites samples.

7.3. FTIR Transmission

This method is very sensible to the functional groups that uptake energy in form of vibration (Smidt, E., et al., 2011). Very small variations of the vibrations forms can be detectable. It is also very sensible to the amount of samples taken, which makes it difficult to quantitative compare two different spectrums.

In order to have a closer approach to a correct comparison of the two FTIR spectrums for each sample, it is necessary to normalize the absorption band areas. The non-carbonated absorption band areas will be used as reference to adjust both spectrums. In order to find a normalizing factor for each sample is needed to find absorptions bands areas that do no present relevant changes before and after carbonation. The area for the absorption bands from the silicate before and after carbonation show a common pattern which is expressed on Area Ratio, in where the compared peaks (V1, V2 y V3) did not change with the carbonate reaction (Table 9). It is possible to conclude that the general area of the absorption silicates bands do not present a relevant variation (Table. 9). Using the ratio for comparison (which is the area ratio average) expressed in Table 9 it is possible to mathematically compare both spectrums for each sample.

Defining a baseline in the V1 until V4 absorptions bands with the program OriginLAB 8, it is possible to calculate the area between the FTIR spectrum and the baseline created (Fig. 18, Fig. B1 – B6).

The area of the V4 absorption band is included on the CO_3^{2-} absorption band due to its relation with the carbonation formation. By normalization of the total areas through the specific area for comparison value, it should be possible to estimate the rate of carbonation and its kinetics for peridotites and carbonates.

Table 9. Area Ratio for the comparison of carbonates absorption bands before and after carbonation for each sample. The peak numbered is shown on the complete FTIR transmission result (Fig. B1 – B6)

	V1 (Area)	V 2 (Area)	V 3 (Area)	Ratio for comparison
LT-1/B/1	1711.37	118.654	5408.86	
LT-1/B	1909.93	131.41	6072.89	1.1154
Area Ratio	1.116	1.107	1.122	
LT-3/B/1	1389.66	108.74	5108.051	
LT-3/B	1651.2143	125.96	5703.153	1.1543
Area Ratio	1.188	1.158	1.116	
LT-4/B/1	2371.97	9531.602	-	
LT-4/B	2177.67	8211.61	-	0.8898
Area Ratio	0.918	0.861	-	
C-626-9/B/1	171.53	806.917	-	
C-626-9/B	135.66	659.917	-	0.8043
Area Ratio	0.791	0.818	-	
14-SC-7/B/1	1546.43	8541.19	-	
14-SC-7/B	1222.96	6356.34	-	1.3041
Area Ratio	1.264	1.344	-	
09-LV-IIA/B/1	3676.72	264.614	-	
09-LV-IIA/B	2940.94	213.231	-	1.2455
Area Ratio	1.2501	1.241	-	

The results do not show a coherent trend. The calculated areas do not reflect the amount of carbonated presented on the sample (Table 10), so it cannot give a quantitative conclusion for carbonation rate. This can be attributed to the complexity of the comparison of different FTIR spectrums

Table 10. Carbonation Rates in percentage after 2 hours of carbonation, obtained through comparison of normalized absorptions bands from the FTIR result before and after carbonation.

			Areas After Carbonation		Normalized Areas After carbonation		Before carbonation	
Sample	Mg #	Ca #	Peak V4	Peak CO_3^{2-}	Peak V4	Peak CO_3^{2-}	Peak CO_3^{2-}	Diference %
LT-1	0.864	0.008	42.2101	62.1700	47.0825	69.3464	87.5034	33.0564
LT-3	0.826	0.033	14.5698	70.9229	16.8188	81.8705	38.5300	156.1361
LT-4	0.805	0.063	3.6380	158.8300	3.2371	141.3269	140.7300	2.7243
C-626-9	0.802	0.199	14.9996	37.4272	12.0650	30.1047	109.8840	-61.6234
14-SC-7	0.804	0.013	6.5227	20.8040	8.5063	27.1308	357.4200	-90.0294
09-LV-IIA	0.800	0.083	28.0370	367.0570	34.9223	457.1986	206.6680	138.1215

The sample 14-SC-7 shows a complex peaks absorptions before carbonation. After carbonation this non-characterized absorptions fade out. This behaviour can be explained by the mineral complexity of the serpentines. On the other hand, the sample 09-LV-IIA shows clear spectrum before and after carbonation.

The samples 14-SC-7 and C-626-9 have a lower area for the carbonation absorption band after the carbonation reaction. This is a non-logical result. The acid triggered de-carbonation experiment results show for these mentioned samples a logical and promising result towards mineral carbonation. The non-logical FTIR results can be attributed to the very small differences of the sample quantity taken for the pellet (Fig. 18, Fig. B1- B6).

The rest of the samples did have more area of the total carbonates absorption bands, but it does not follow a recognisable pattern. The samples who present the greater positive area variation are LT-3, followed by 09-LV-IIA.

The V4 absorption band area, which correspond to the characteristic C=O functional group, only appears after carbonation reaction in every single sample. The values of this area have a direct relation to the carbonates formation that took place. There is no need for comparison between the two spectrums for each sample, which reduces probable uncertainties. It should be taken into account that comparing the spectrums of the different samples should be done by area normalization, nevertheless this cannot be done in this thesis because the mineralogical differences between different samples. Therefore this area can qualitative estimate the carbonation rate.

The sample who presents the most V4 area is the LT-1, who has the bigger Mg# and the lower Ca#. Therefore LT-1 has the greater carbonation rate. The sample who has the lower carbonation rate is the LT-4. Serpentines samples have a complicated behaviour where the carbonation rate presents steeper variation with minimal Mg# and Ca# changes.

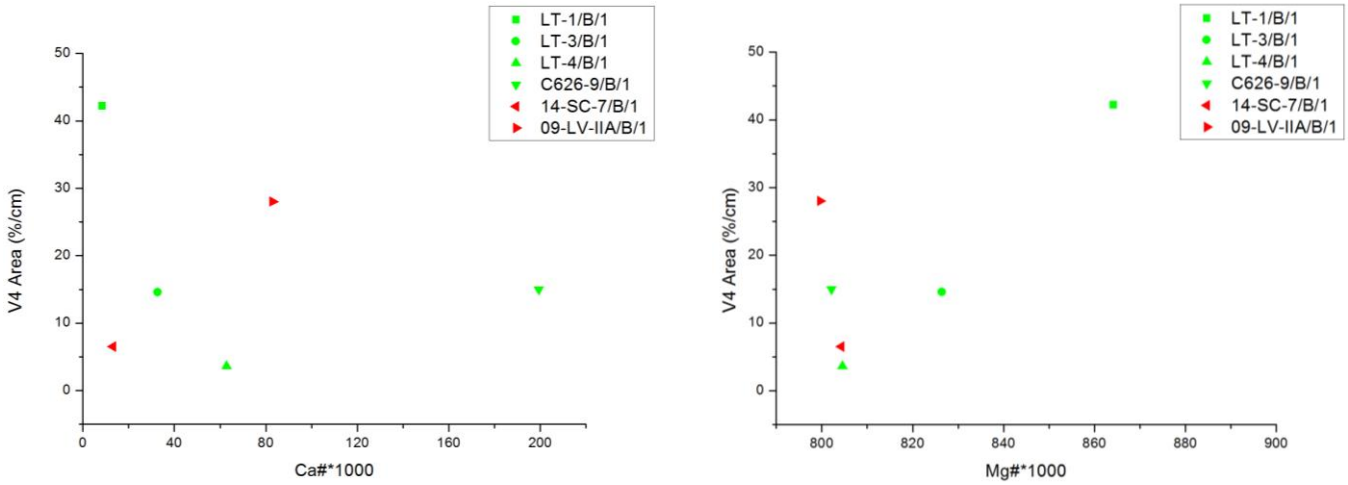

Fig. 20. Comparison between the V4 absorbance normalized area of the samples after carbonation and the (Left) Ca# with a two parameter exponential function (Exp2P) and (Right) Mg# with a three parameter exponential function (Exp3P2). The non-linear curves were calculated with OriginLab 8. Green: Peridotites samples, Red: Serpentines samples.

By comparing the V4 absorption band area with the correspondent Ca# and Mg# of the peridotites samples it is possible to find a carbonation reaction trend, similar to the resultant one with the acid triggered de-carbonation experiment (Fig. 19, Fig. 20). Serpentine samples are excluded on the non-linear fitted curve calculation because its complex behaviour towards carbonation reaction. These results confirm the inverse relation of Mg# and Ca# towards mineral carbonation. At higher Mg# the bigger the mass loss %, and at higher Ca#, the lower the mass loss. There is still a lot of work to do regarding the influence of Mg# and Ca# as a factor for carbonation of peridotites and serpentines.

FTIR transmission results reveal the carbonation formation that has taken place on the reactor at 185ºC and a constant CO_2 pressure of 1 atm for 2 hours. Additionally, the characteristic doublet of the asymmetric C-O stretching mode of magnesite (Turianicová, E., et al., 2013, Nichols, A., and Wysoczanski, R., 2007; Zhang, Z., et al., 2006) is recognizable for all the samples after carbonation reaction. The latter revealed the Magnesite formation under this thesis set up conditions. Nevertheless its formation rate cannot be quantitatively analysed with the methods used in this study.

8. Conclusions

FTIR, XRD and acid triggered de-carbonation results have proved that under this thesis conditions (based on the paper Kelemen and Matter, 2008) the formation of carbonates of peridotites and serpentines occurred. Nevertheless, none of these three methods could give a quantitatively precise carbonation rate and its kinetics.

FTIR is a very sensitive method, and can detect little variations on functional groups that uptake energy in form of vibration. Because this sensibility, it is very easy to recognize small variations of the analysed samples. On the other hand, an accurate quantitative comparison of different spectrums could be challenging and imprecise. This method results revealed the carbonation formation by CO_2 uptake has occur in all the samples. The latter gave the most accurate carbonation formation response. The mineral carbonation formation is mainly quantified by the typical C=O absorption band presented in all the samples only after carbonation. Magnesite characteristic double peak absorption is easier to identify on the samples exposed to carbonation conditions. Therefore, Magnesite has also formed under this thesis conditions.

XRD result shows an increase of Calcite in all the peridotites samples. Dolomite and Magnesite do not present a recognizable logical variation. Olivine and serpentines mineral proportions vary, revealing its affinity towards carbonation reaction. It is not possible to determine under this conditions which reactant mineral has contributed the most towards CO_2 sequestration. This method is imprecise at very low mineral changes. Therefore it cannot guarantee under these conditions a precise proportional mineral comparison before and after carbonation.

The acid triggered experiment result revealed CO_2 uptake by mineral carbonation, reaching a maximum carbonation rate of 4%. This experiment is imprecise due to the possible measure differences due to the human factor. On the other hand, it is very handy in order to give a qualitative result.

Acid triggered de-carbonation and FTIR transmission results revealed an inverse relation between Mg# and Ca# towards carbonation. At higher Mg# higher rate of carbonation is obtained. The Dunite sample (LT-1) has carbonated the most of the peridotites samples, which is the sample that has the highest Mg# and the lower Ca#. The full quantification of Mg# and Ca# influence towards CO_2 uptake of peridotites and serpentines remains a future challenge.

Serpentine samples have complicated responses obtained by different methods. It may be because its mineralogical complexity and their pre-existing carbonates. It was not possible to accurately estimate a carbonation rate or/and trend based on its composition.

Further investigations are required in order to enhance the carbonation rate with low cost energy processes. Peridotites carbonation is a complicated phenomenon due to simultaneous chemical and morphological grain changes. In order to enhance the peridotites and serpentines CO_2 uptake, it is important to understand the reaction mechanisms and kinetics. Many experiments at optimal carbonation conditions needs to be done in a quantitative way to feasibly enhance the carbonation rate, such as development of feasible peridotites and serpentines nanomaterials by ball milling with ethanol, proposed at Rigopoulos, I., et. al., 2015b, fluid interaction with ultramafic samples proposed at Kelemen and Matter, 2008, considerably adding $NaHCO_3$ to the solution (i.e.: Gadikota, G., et al., 2014) and sample *heat*-pretreatment (i.e.: Turinacová, E., et. al., 2013).

9. References

Béarat, H., Michael, J. M., Chizmeshya, A. V. G., Gormley, D., Nuñez, R., Carpenter, R. W., … Wolf, G. H. (2006). Carbon Sequestration via Aqueous Olivine Mineral Carbonation: Role of passivating Layer Formation. **Environmental Science & Technology, 40**, pp. 4802–4808.

Bishop, J. L., Perry, K. A., Darby Dyar, M., Bristow, T. F., Blake, D. F., Brown, A. J., & Peel, S. E. (2013). Coordinated spectral and XRD analyses of magnesite-nontronite-forsterite mixtures and implications for carbonates on Mars. **Journal of Geophysical Research E: Planets, 118(4)**, 635–650.

Böttcher, M. E., & Gehlken, P. L. (1995). Cationic substitution in natural siderite-magnesite (FeCO3-MgCO3) solid-solutions: A FTIR spectroscopic stuy. **Neues Jahrbuch Für Mineralogie - Abhandlungen-**, *169*, 81–95.

Bruckman, V. J., & Wriessnig, K. (2013). Improved soil carbonate determination by FT-IR and X-ray analysis. **Environmental Chemistry Letters, 11(1)**, 65–70.

Chizmeshya, A. V. G., McKelvy, J. M., Squires, K., Carpenter, R. W., & Béarat, H. (2007). A Novel Approach to Mineral Carbonation: Enhancing Carbonation While Avoiding Mineral Pretreatment Process Cost. **U.S. Dep. Energy Final Report 924162**. Arizona State University. Arizona.

Coates, J. (2000). Interpretation of Infrared Spectra, A Practical Approach. ***Encyclopedia of Analytical Chemistry***, 10815–10837.

Draper, G. (2006). Ophiolite-Related Ultramafic Rocks (Serpentinites) in the Caribbean Region : a Review of their Occurrence , Composition , Origin , Emplacement and Ni-Laterite Soil Formation. **Geological Acta, 4 (1-2)**, 237-263.

Duke, D. a, & Stephens, J. D. (1964). Infrared investigation of the olivine group minerals. **American Mineralogist, 49**, 1388.

Escuder Viruete, J., Díaz de Neira, A., Hernáiz Huerta, P. P., Monthel, J., Senz, J. G., Joubert, M., … Pérez-Estaún, A. (2006). Magmatic relationships and ages of Caribbean Island arc tholeiites, boninites and related felsic rocks, Dominican Republic. **Lithos, 90(3-4)**, 161–186.

Frost, B. R., & Beard, J. S. (2007). On Silica Activity and Serpentinization. **Journal of Petrolgy, 48(7)**, 1351–1368.

Gadikota, G., Matter, J., Kelemen, P., & Park, A.-H. A. (2014). Chemical and morphological changes during olivine carbonation for CO2 storage in the presence of NaCl and NaHCO3. **Physical Chemistry Chemical Physics : PCCP, 16(10)**, 4679–93.

Garrido, C. J., Bach, W., Gervilla, F., & Gonzáles, J. M. (2006). Descifrando la Secuencia de Serpentinizacion en Peridotitas de la Dorsal del Océano Atlántico (ODP Leg 209, lat. 150N). **Macla, 6**, 2004–2007.

Gerdemann, S. J., Dahlin, D. C., O'Connor, W. K., & Penner, L. R. (2003). Carbon Dioxide Sequestration by Aqueous Mineral Carbonation of Magnesium Silicate Minerals.

Greenhouse Gas Technologies, (US Albany Research Center (ARC)) Albany OR, p.8. **Proceedings of the Second Annual Conference on Carbon Sequestration**, 5-9 May 2003, Alexandria, VA, USA.

Global CCS Institute. (2015). **The global Status of CCS | 2015: Summary Report**. Melbourne.

Golightly, J. P., & Arancibia, O. N. (1979). The chemical composition and infrared spectrum of nickel and iron-substituted serpentine from a nickeliferous laterite profile, Soroako, Indonesia. **Canadian Mineralogist, 17**, 719–728.

Hamilton, V. E. (2000). Thermal infrared emission spectroscopy of the pyroxene mineral series. **Journal of Geophysical Research, 105(E4)**, 9701.

Hänchen, M., Prigiobbe, V., Baciocchi, R., & Mazzotti, M. (2008). Precipitation in the Mg-carbonate system-effects of temperature and CO2 pressure. **Chemical Engineering Science, 63(4)**, 1012–1028.

Hansen, L. D., Dipple, G. M., Gordon, T. M., & Kellett, D. A. (2005). Carbonated Serpentinite (Listwanite) at Atlin, British Columbia: A Gelological Analogue to Carbon Dioxide Sequestration. **The Canadian Mineralogist, 43**, 225–239.

IEA. (2013a). **Global Action to Advance Carbon Capture and Storage: A focus on Industrial Applications: Annex to Tracking Clean Energy Progress 2013**. Paris.

IEA. (2013b). **Technology Roadmap: Carbon Capture and Storage**. Paris.

IEA. (2015a). **Carbon Capture and Storage : The solution for deep emissions reductions**. Paris.

IEA. (2015b). **Energy Technology Perspectives 2015: Executive Summary: Mobilising Innovation to Accelerate Climate Action**. Paris.

IPCC. (2005). Special Report on Carbon Dioxide Capture and Storage. **Prepared by Working Group III of the intergovernamental Panel on Climate Change**. Cambridge, UK and NY.

IPCC. (2013). Summary for Policymarkers. In: Climate Change 2013: The Physical Scinece Basis. **Contribution of Working Group I to the Fifth Assessment Report of the Intergovernmental Panel on Climate Change**. Cambridge, UK and NY.

IPCC. (2014). Climate Change 2014 Synthesis Report. **Contribution of Working Groups I, II, III to the Fifth Assesment Resport of the Intergovernmental Panel on Climate Change**. Geneva.

Jagoutz, E., Palme, H., Baddenhausen, H., Blum, K., Cendales, M., Dreibus, G., … Vanke, H. (1979). The abundance of major, minor and trace elements in the earth ' s mantle as derived from primitive ultramafic nodules. **Geochimica et Cosmochimica Acta, 11(March)**, 2031–2050.

Kelemen, P. B., & Matter, J. (2008). In situ carbonation of peridotite for CO 2 storage. **PNAS, 105(45)**, 17295–17300.

Klein, F., & Garrido, C. J. (2011). Thermodynamic constrains on mineral carbonation of serpentinized peridotite. **Lithos, 126(OCTOBER)**, pp. 147–160.

Lafay, R., Montes-Hernandez, G., Janots, E., Chiriac, R., Findling, N., & Toche, F. (2012). Mineral replacement rate of olivine by chrysotile and brucite under high alkaline conditions. **Journal of Crystal Growth, 347(1)**, 62–72.

Lafay, R., Montes-Hernandez, G., Janots, E., Chiriac, R., Findling, N., & Toche, F. (2014). Simultaneous precipitation of magnesite and lizardite from hydrothermal alteration of olivine under high-carbonate alkalinity. **Chemical Geology, 368**, 63–75.

Lafuente B, Downs R T, Yang H, Stone N (2015). The power of databases: the RRUFF project. In: Highlights in Mineralogical Crystallography, **Armbruster, T.m and Danisi, R.M., eds.** Berlin, Germany, W. De Gruyter, pp 1-30

Lewis, J. F., Draper, G., Proenza, J. A., Espaillat, J., & Jiménez, J. (2006). Ophiolite-related ultramafic rocks (serpentinites) in the Caribbean region: A review of their occurrence, composition, origin, emplacement and Ni-laterite soil formation. **Geologica Acta, 4(1-2)**, 237–263.

Malvoisin, B. (2015). Mass transfer in the oceanic lithosphere: {Serpentinization} is not isochemical. **Earth and Planetary Science Letters, 430**, 75–85.

Marchesi, C., Garrido, C. J., Proenza, J. A., Hidas, K., Varas-Reus, M. I., Butjosa, L., & Lewis, J. F. (2016). Geochemical record of subduction initiation in the sub-arc mantle: Insights from the Loma Caribe peridotite (Dominican Republic). **Lithos, 252-253(April 2016)**, 1–15.

Melgarejo, J. C., Proenza, J. A., Galí, S., & Llovet, X. (2010). Técnicas de caracterización mineral y su aplicación en exploración y explotación minera. **Boletin de La Sociedad Geologica Mexicana**, *62*(1), 1–23.

Mellini, M., Fuchs, Y., Viti, C., Lemaire, C., & Linarès, J. (2002). Insights into the antigorite structure from Mössbauer and FTIR spectroscopies. **European Journal of Mineralogy, 14(1)**, 97–104.

Neubeck, A., Duc, N. T., Hellevang, H., Oze, C., Bastviken, D., Bacsik, Z., & Holm, N. G. (2014). Olivine alteration and H2 production in carbonate-rich, low temperature aqueous environments. **Planetary and Space Science, 96**, 51–61.

Nichols, A. R. L., & Wysoczanski, R. J. (2007). Using micro-FTIR spectroscopy to measure volatile contents in small and unexposed inclusions hosted in olivine crystals. **Chemical Geology, 242(3-4)**, 371–384.

O'Connor, W. K., Dahlin, D. C., Rush, G. E., Gerdemann, S. J., Penner, L. R., & Nilsen, D. N. (2005). Final Report: Aqueous Mineral Sequestration. **Office of Process Development, National Energy Technology Laboratory**, formerly Albany Research Center, Office of Fossil Fuel Energy, US DOE.

Omori, K. (1971). Analysis of the infrared absorption spectrum of diopside. **The American Mineralogist, 56**, 1607–1616.

Pecharsky, V., & Zavalij, P. Y. (2005). Fundamentals of Powder Diffraction and Structural Characterization of Materials. Library of Congress Cataloging-in-Publication data. **QC482.D5P43, 548'.83-dc22, SPRINGER**, New York.

Reig, F. B., Adelantado, J. V. G., & Moya Moreno, M. C. M. (2002). FTIR quantitative analysis of calcium carbonate (calcite) and silica (quartz) mixtures using the constant ratio method. Application to geological samples. **Talanta, 58(4)**, 811–821.

Rigopoulos, I., Petallidou, K. C., Vasiliades, M. A., Delimitis, A., Ioannou, I., Efstathiou, A. M., & Kyratsi, T. (2015a). Carbon Dioxide Dtorage in Olivine Basalts : Effect of Ball Milling Process. **Powder Technology, 273(October)**, pp. 220–229.

Rigopoulos, I., Vasiliades, M. A., Petallidou, K. C., Ioannis, I., Efstathiou, A. M., & Kyratsi, T. (2015b). A method to enhance the CO 2 Storage capacity of pyroxenitic rocks. **Greenhouse Gases: Science and Technology, 5,** 1–14.

Saikia, B. J., Parthasarathy, G., & Sarmah, N. C. (2009). Spectroscopic Characterization of Olivine [(Fe , Mg) 2 SiO 4] in Madadevpur H4 / 5 ordinary chondrite. **Science, 5(4)**, 71–78.

Santos, R., Van Audenaerde, A., Chiang, Y., Iacobescu, R., Knops, P., & Van Gerven, T. (2015). Nickel Extraction from Olivine: Effect of Carbonation Pre-Treatment. **Metals, 5(3)**, 1620–1644.

Schuiling, R. D., & Krijgsman, P. (2006). Enhanced Weathering: An Effective and Cheap Tool to Sequester CO2. **Climate Change, 74(nrs 1-3)**, pp. 349–354.

Sissmann, O., Brunet, F., Martinez, I., Guyot, F., Verlaguet, A., Pinquier, Y., & Daval, D. (2014). Enhanced olivine carbonation within a basalt as compared to single-phase experiments: Reevaluating the potential of CO2 mineral sequestration. **Environmental Science and Technology, 48(10)**, 5512–5519.

Smidt, E., Böhm, K., & Schwanninger, M. (2011). The application of FT-IR spectroscopy in waste management, in: G. Nikolic (Ed.), Fourier Transforms - New Analytical Approaches and FTIR Strategies, **InTech 2011**, pp 405–430.

Streit, E., Kelemen, P., & Eiler, J. (2012). Coexisting Serpentine and Quartz from Carbonate-Bearing Serpentinized Peridotite in the Samail Ophiolite , Oman. **Contribution to Mineralogy and Petrology, 164(5)**, pp. 821–837.

Stuart, B. H. (2004). *Infrared Spectroscopy: Fundamentals and Applications*. Analytical Techniques in the Sciences, Willey (Ed.), **Methods (Vol. 8)** pp. 224

Turianicová, E., Baláz, P., Tucek, Lubomír, Zorkovská, A., Zelenák, V., Németh, Z., … Kovác, J. (2013). A comparison of the reactivity of activated and non-activated olivine with CO2. **International Journal of Mineral Processing, 123(September)**, 73–77.

Willis, R., Spencer, M., Metternich, F., Crane, K., Jacobs, M., Morgan, G., … Pumphrey, K. (2014). Paris 2015. **Getting a global agreement on climate change, 1–24.**

Xu, T., Apps, J. A., & Pruess, K. (2004). Numerical Simulation of CO2 Disposal by Mineral Trapping in Deep Aquifers. **Applied Geochemistry, 19**, 917–936.

Zhang, Z., Zheng, Y., Ni, Y., Liu, Z., Chen, J., & Liang, X. (2006). Temperature- And pH-dependent morphology and FT-IR analysis of magnesium carbonate hydrates. **Journal of Physical Chemistry B, 110(26)**, 12969–12973.

9.1. Newspaper References

Bill McKibben (December 13th, 2015). Climate deal: The pistol has fired, so why aren't we running?. **The Guardian.**

Arthur Neslen in Brevik, Norway. April the 9th, 2015. Europe's carbon capture dream beset by delays, fears and doubt. **The Guardian.**

10. Appendix A

10.1. X-Ray Powder Diffraction of the sample before carbonation

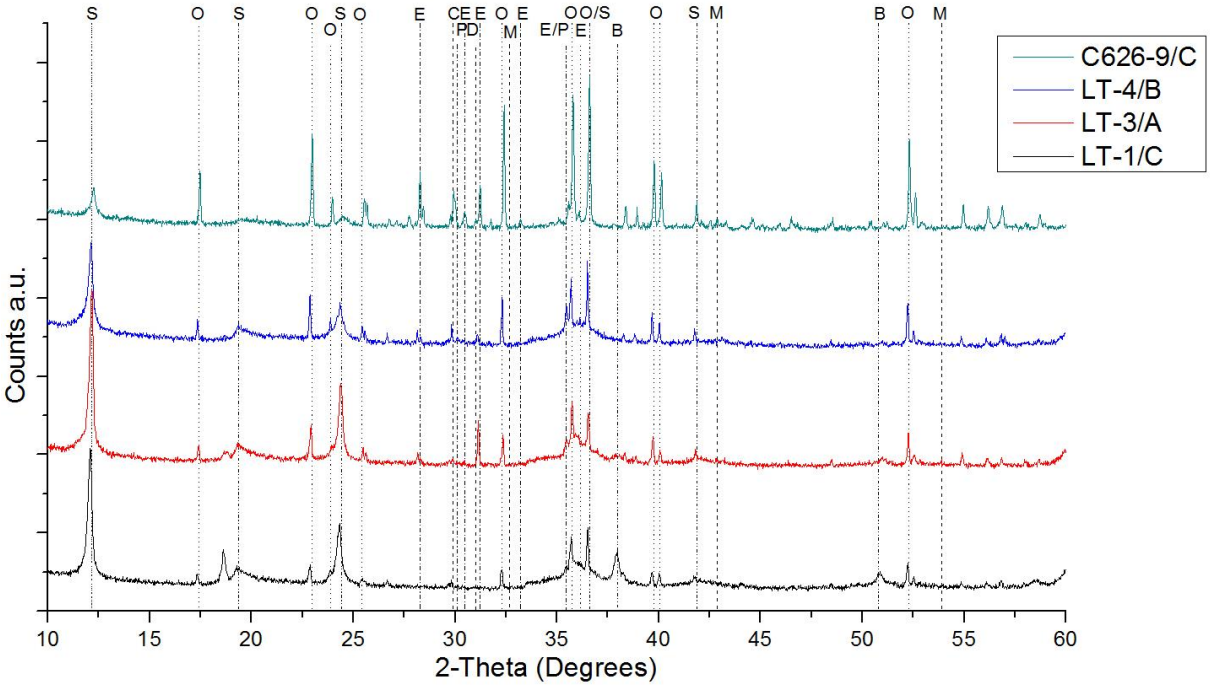

Fig. A 1. Results of the X-Ray Powder Diffraction analysis from 2θ = 10º - 40º and interpretation of the peridotites samples; S: Serpentine, O: Olivine, P: Clinopyroxene, E: Orthopyroxene, D: Dolomite; C: Calcite, M: Magnesite, B: Brucite.

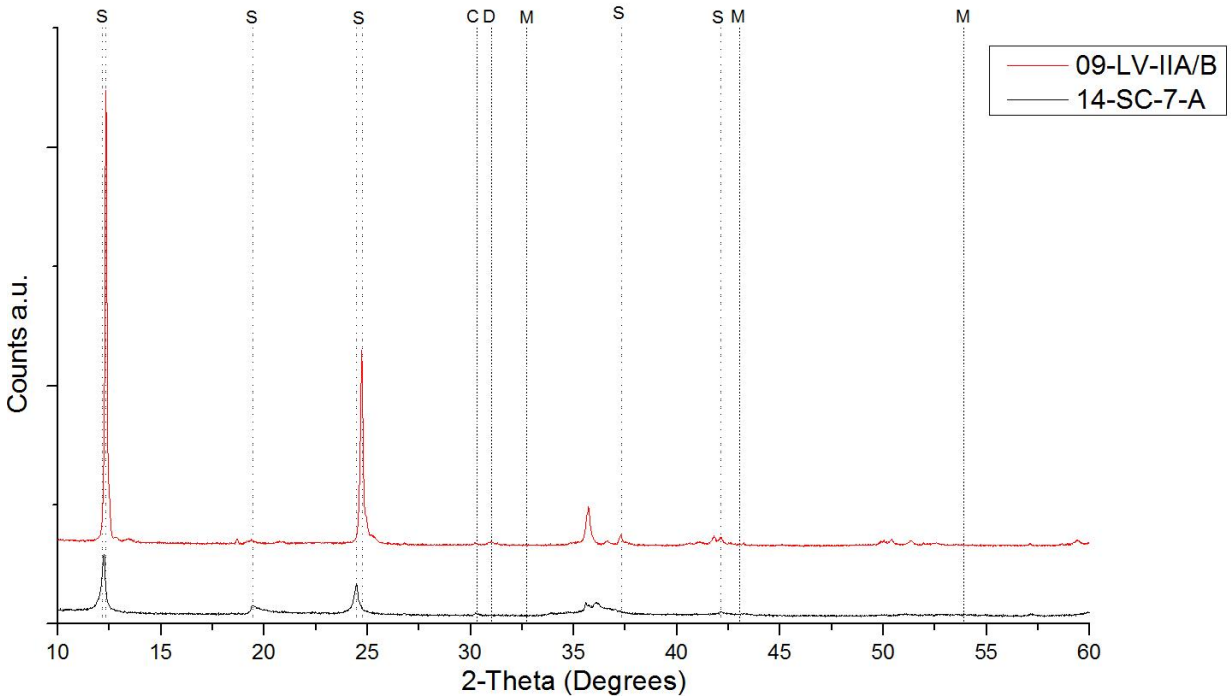

Fig. A 2. Results of the X-Ray Powder Diffraction analysis from 2θ = 10º - 60º and interpretation of the Serpentine samples; S: Serpentine, O: Olivine, C: Calcite; M: Magnesite; D: Dolomite. The peak counts for the sample 09-LV-IIA are much higher than the ones from 14-SC-7.

10.2. X-Ray Powder Diffraction of the samples before and after carbonation targeting the 100 peaks for Carbonates, Serpentine and Silicates.

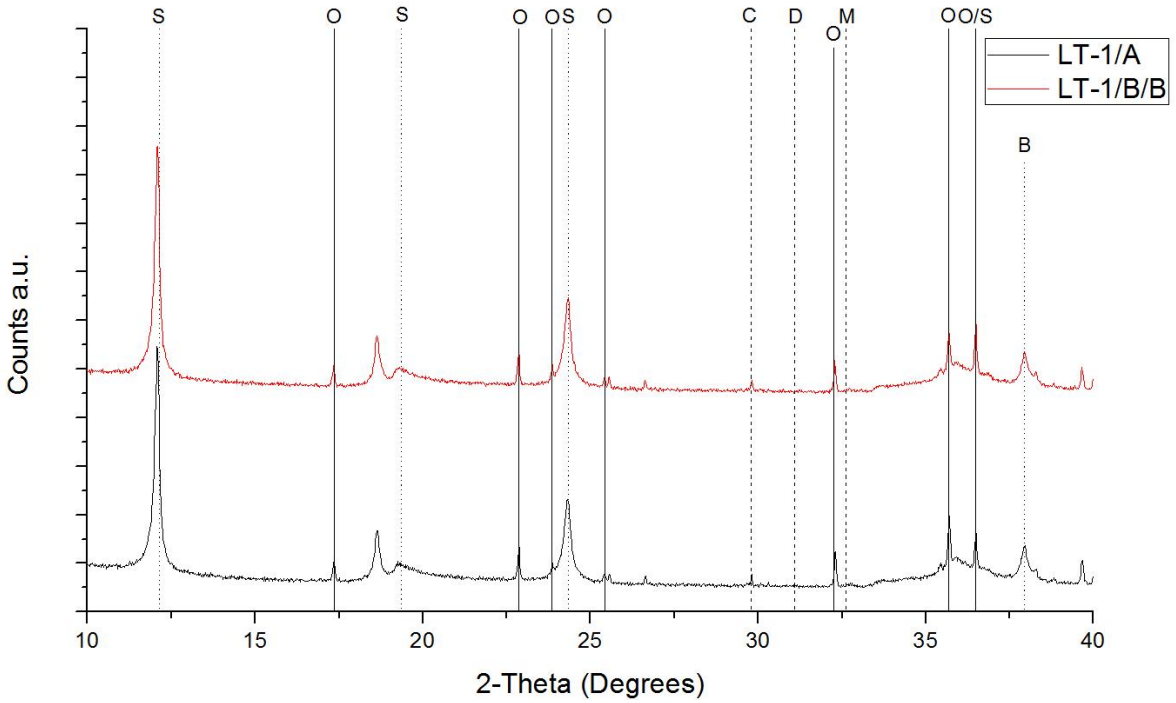

Fig. A3. Results of the X-Ray Powder Diffraction analysis from 2θ = 10º - 40º targeting the 100 peaks for Carbonates, Serpentine and Silicates of the LT-1 samples before and after carbonation. S: Serpentine, O: Olivine, D: Dolomite; C: Calcite, M: Magnesite, B: Brucite.

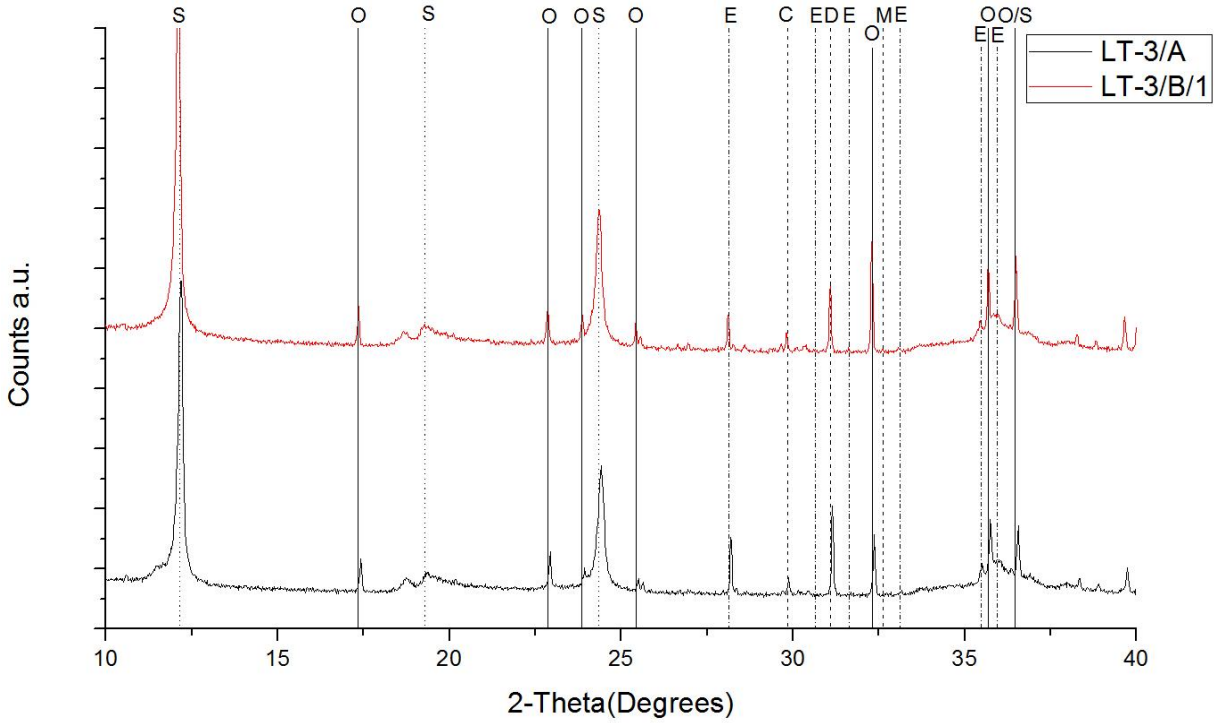

Fig. A4. Results of the X-Ray Powder Diffraction analysis from 2θ = 10º - 40º targeting the 100 peaks for Carbonates, Serpentine and Silicates of the LT-3 samples before and after carbonation. S: Serpentine, O: Olivine, E: Orthopyroxene, D: Dolomite; C: Calcite, M: Magnesite.

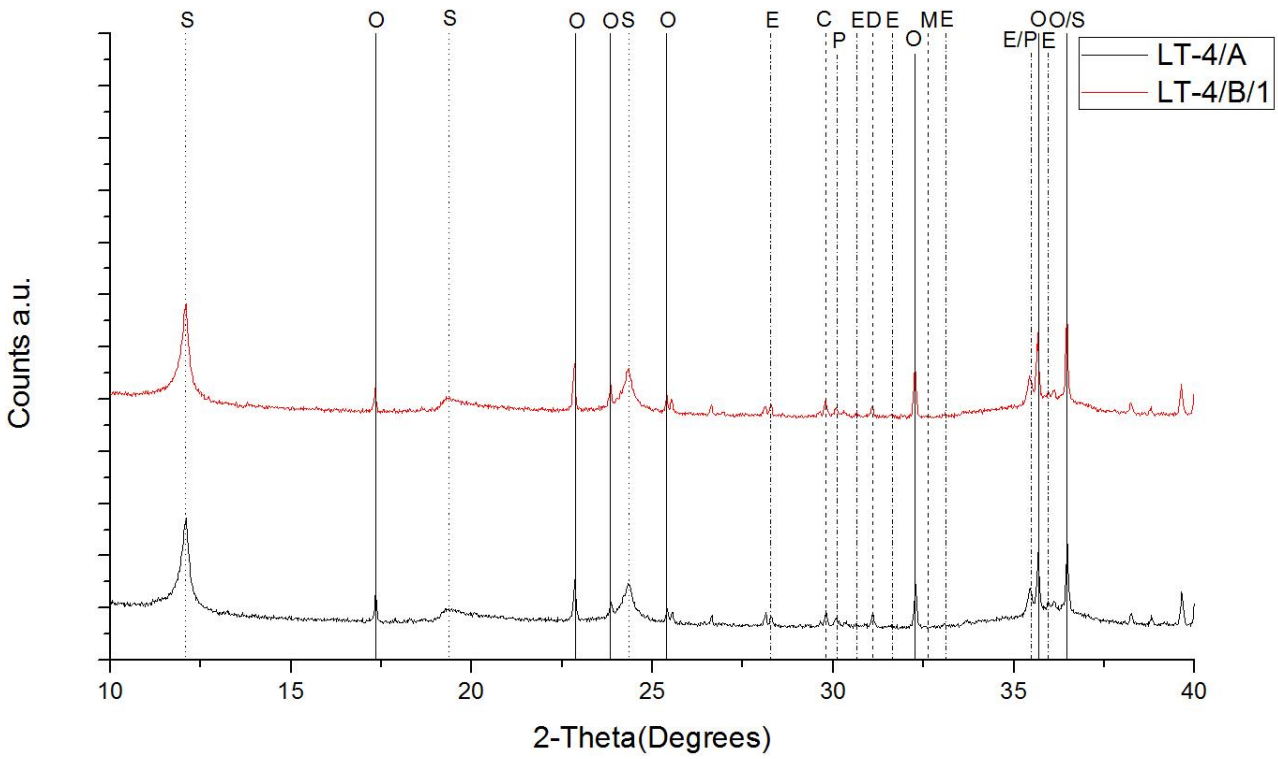

Fig. A5. Results of the X-Ray Powder Diffraction analysis from 2θ = 10º - 40º targeting the 100 peaks for Carbonates, Serpentine and Silicates of the LT-4 samples before and after carbonation. S: Serpentine, O: Olivine, P: Clinopyroxene, E: Orthopyroxene, D: Dolomite; C: Calcite, M: Magnesite.

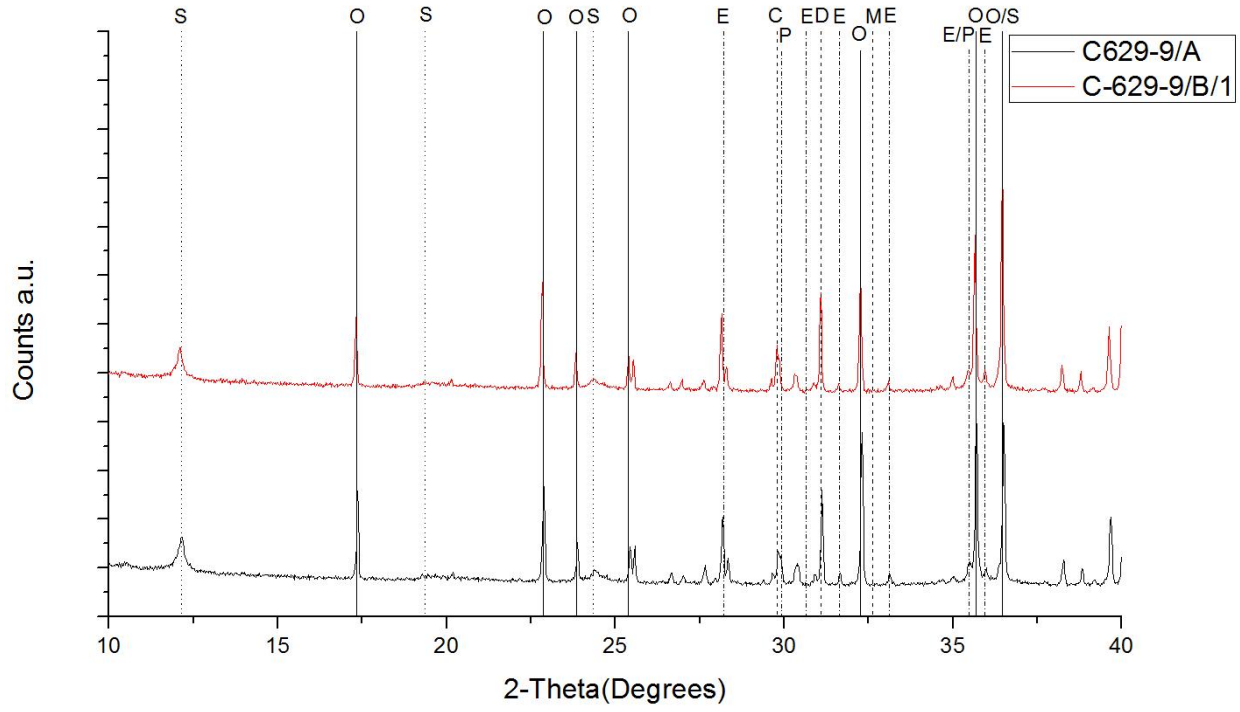

Fig. A6. Results of the X-Ray Powder Diffraction analysis from 2θ = 10º - 40º targeting the 100 peaks for Carbonates, Serpentine and Silicates of the C-626-9 samples before and after carbonation. S: Serpentine, O: Olivine, P: Clinopyroxene, E: Orthopyroxene, D: Dolomite; C: Calcite, M: Magnesite.

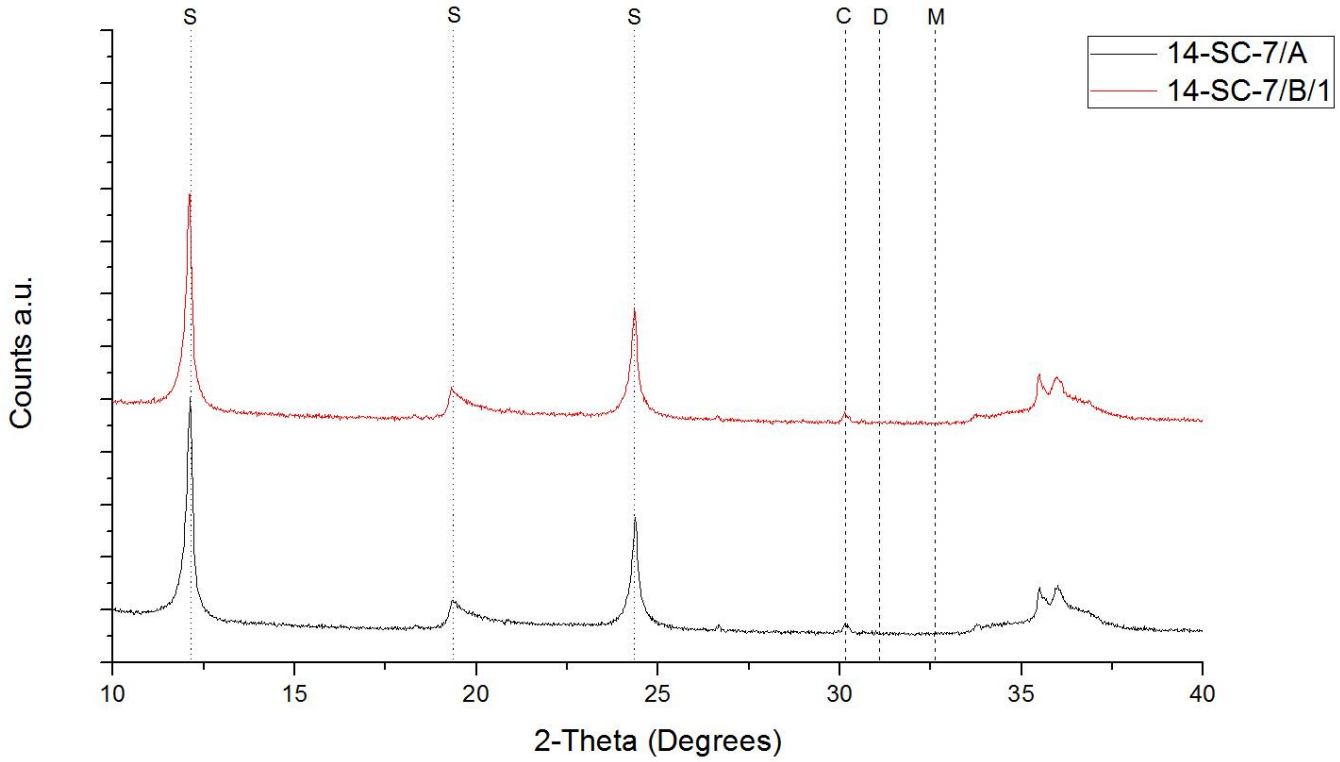

Fig. A7. Results of the X-Ray Powder Diffraction analysis from 2θ = 10º - 40º targeting the 100 peaks for Carbonates, Serpentine and Silicates of the 14-SC-7 samples before and after carbonation. S: Serpentine, D: Dolomite; C: Calcite, M: Magnesite.

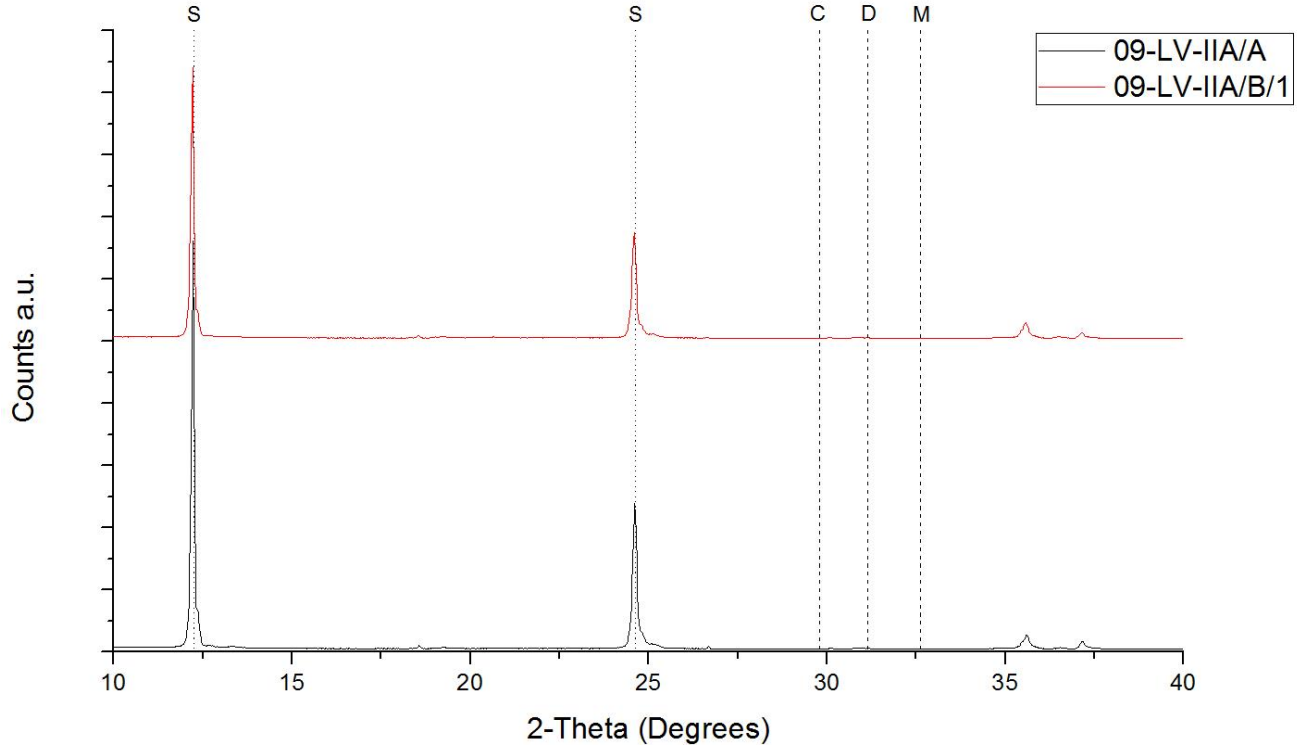

Fig. A8. Results of the X-Ray Powder Diffraction analysis from 2θ = 10º - 40º targeting the 100 peaks for Carbonates, Serpentine and Silicates of the 09-LV-IIA samples before and after carbonation. S: Serpentine, D: Dolomite; C: Calcite, M: Magnesite.

11. Appendix B

11.1. FITR Transmission results (Before and after carbonation)

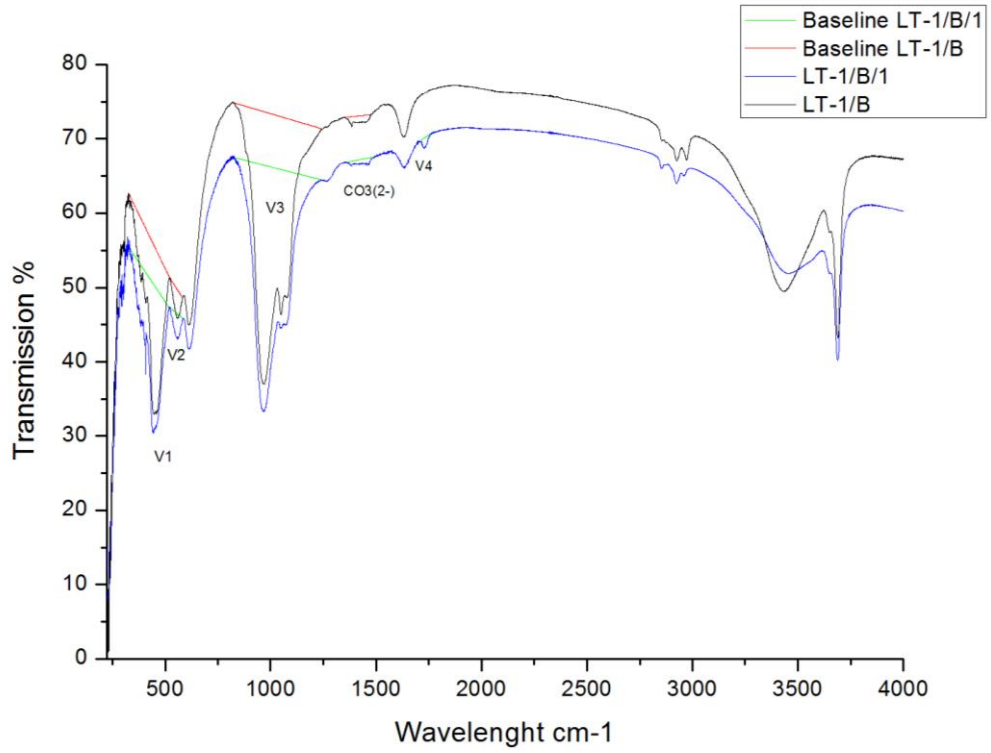

Fig. B1. FTIR transmission spectrum result of the sample LT-1 before and after carbonated. The V indicates the peaks use for comparison, and the base line determines the area to be calculated.

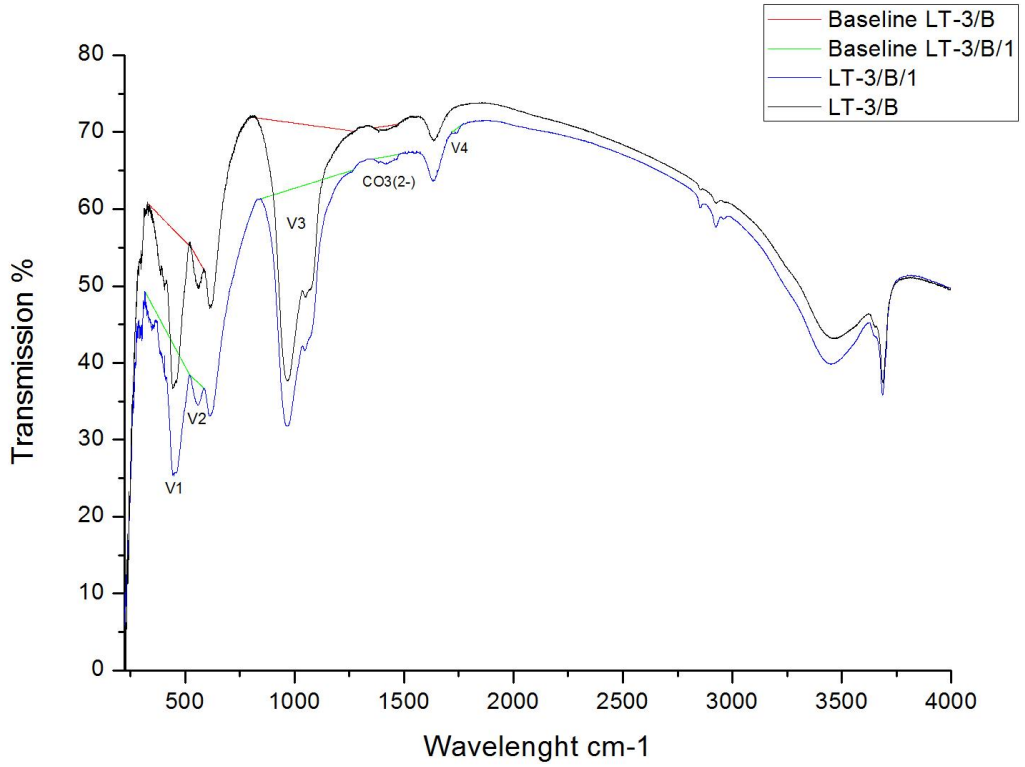

Fig. B2. FTIR transmission spectrum result of the sample LT-3 before and after carbonated. The V indicates the peaks use for comparison, and the base line determines the area to be calculated.

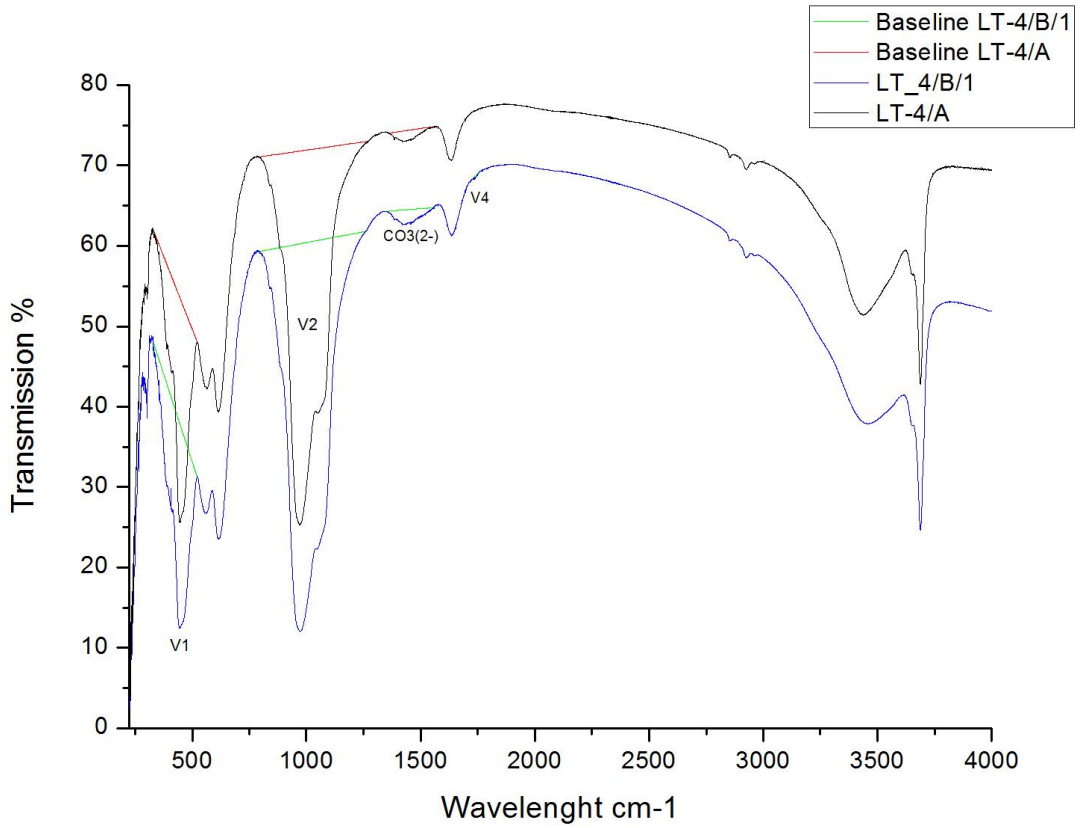

Fig. B3. FTIR transmission spectrum result of the sample LT-4 before and after carbonated. The V indicates the peaks use for comparison, and the base line determines the area to be calculated.

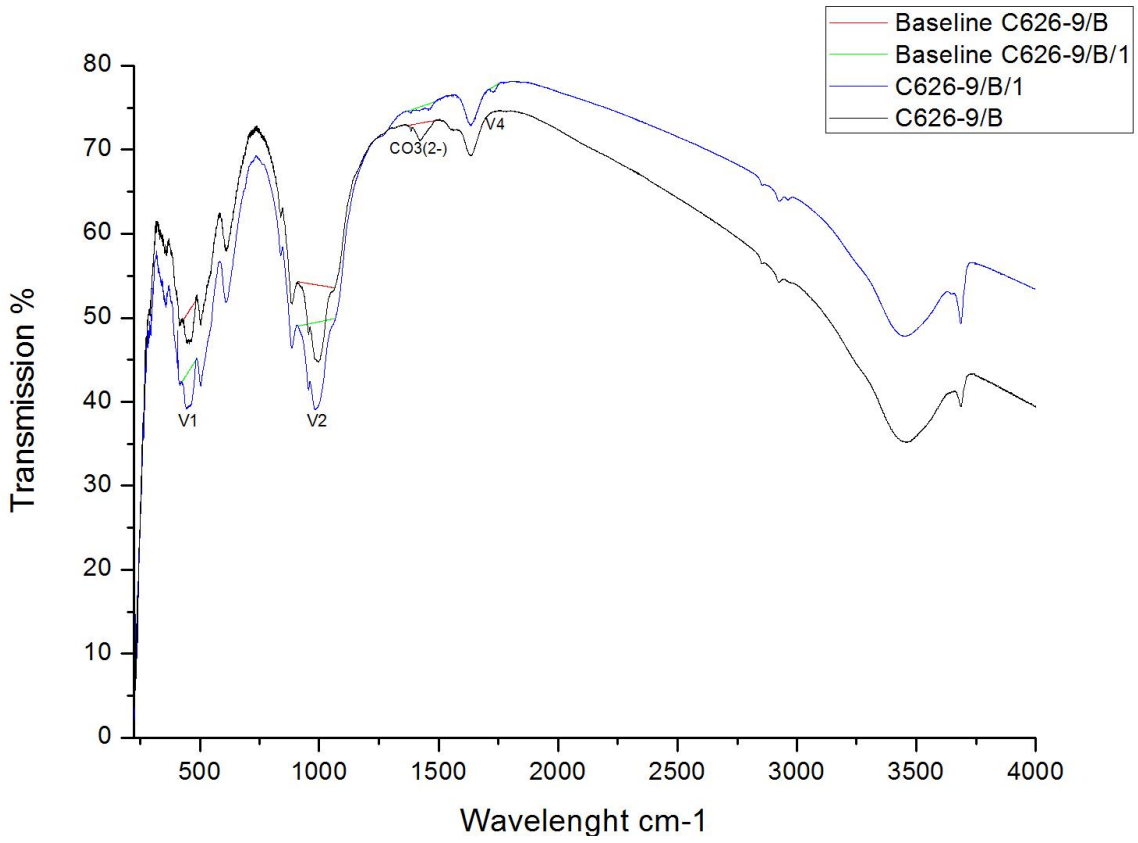

Fig. B4. FTIR transmission spectrum result of the sample C-626-9 before and after carbonated. The V indicates the peaks use for comparison, and the base line determines the area to be calculated.

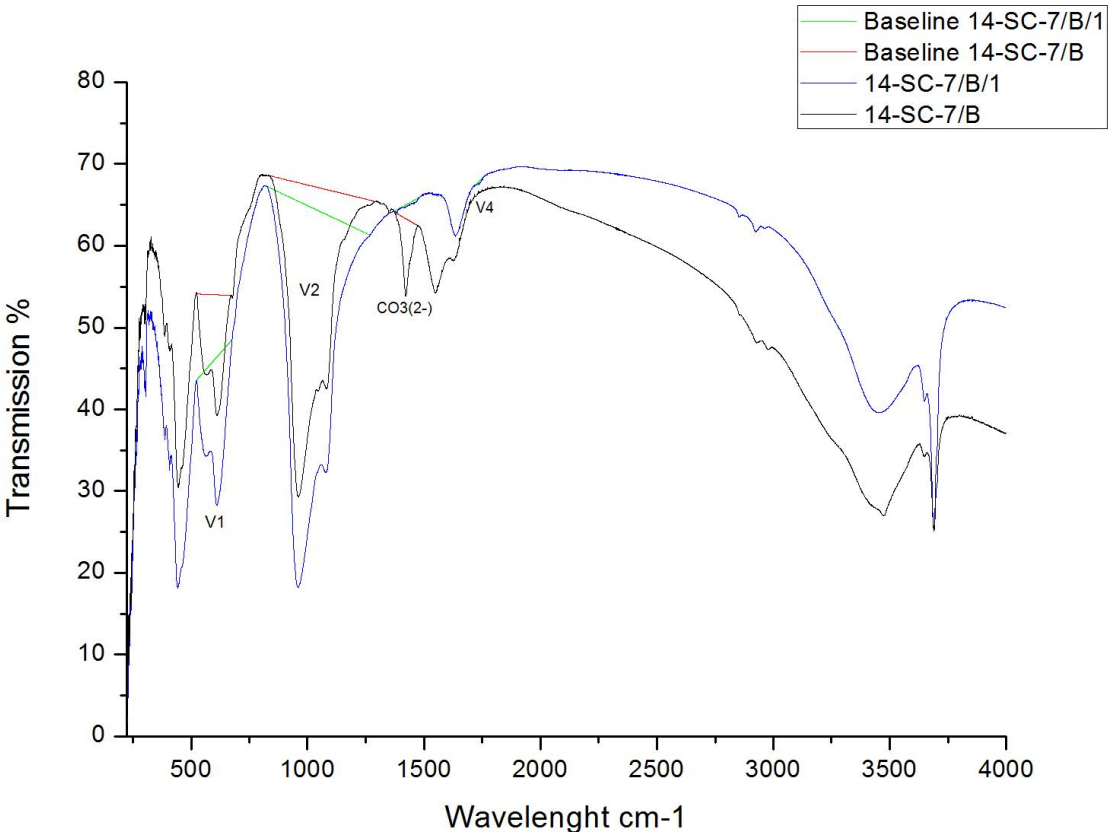

Fig. B5. FTIR transmission spectrum result of the sample 14-SC-7 before and after carbonated. The V indicates the peaks use for comparison, and the base line determines the area to be calculated.

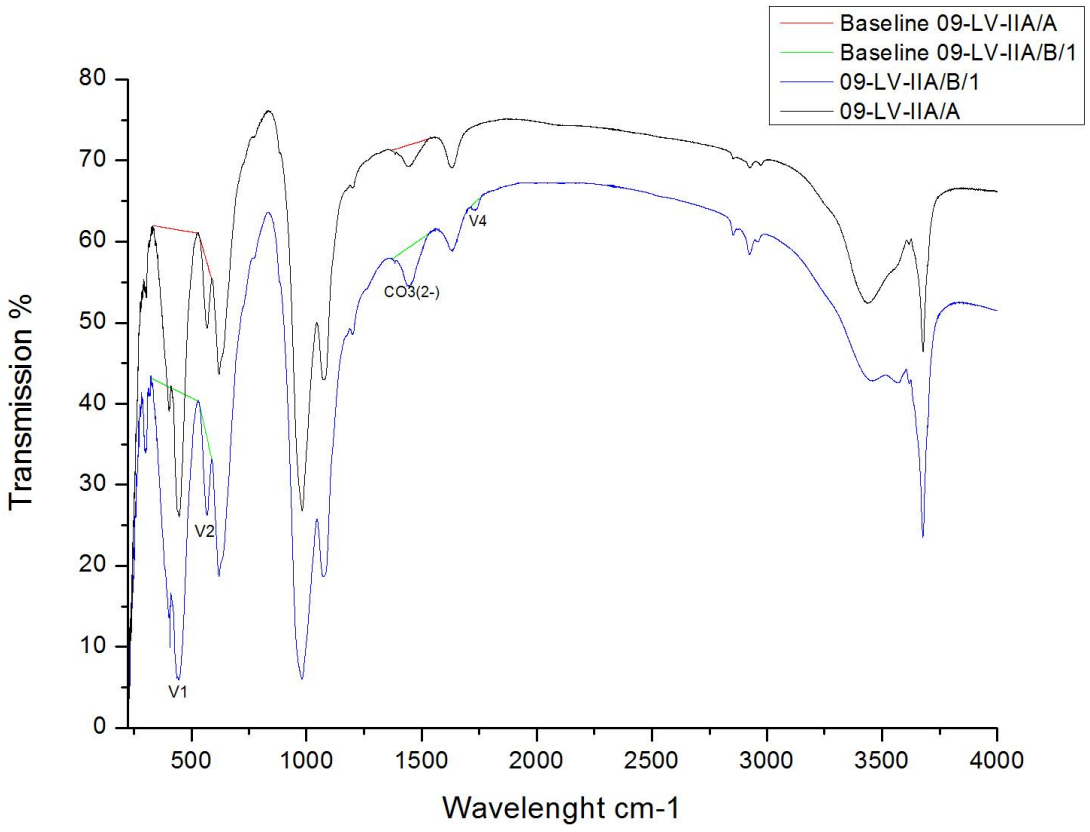

Fig. B6. FTIR transmission spectrum result of the sample 09-LV-IIA before and after carbonated. The V indicates the peaks use for comparison, and the base line determines the area to be calculated.